JCI The Journal of Clinical Investigation

Neutrophil extracellular traps induced by chemotherapy inhibit tumor growth in vivo

Yamu Li, … , David L. Bajor, Zhenghe Wang

J Clin Invest. 2024. https://doi.org/10.1172/JCI175031.

Research In-Press Preview Oncology

Graphical abstract

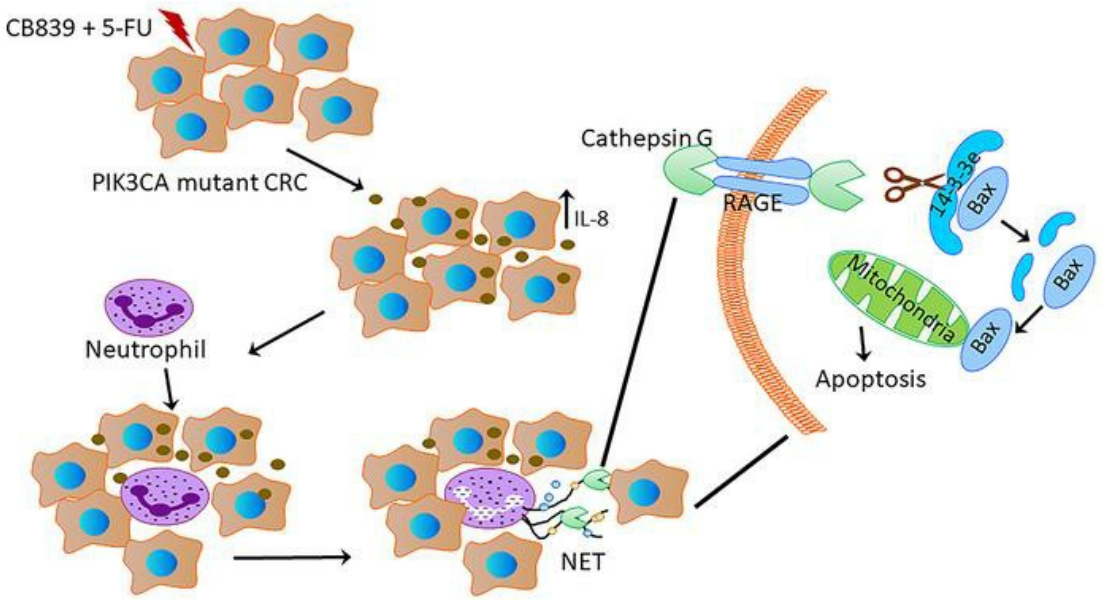

Neutrophil Extracellular Traps induced by chemotherapy inhibit tumor growth in murine models of colorectal cancer

Yamu Li[1,2], Sulin Wu[1,3,4], Yiqing Zhao[1,2], Trang Dinh[1,2], Dongxu Jiang[1,2], Eva Selfridge[1,2,3,5], George Myers[6], Yuxiang Wang[1,2], Xuan Zhao[1,2], Suzanne Tomchuck[7], George Dubyak[8], Richard Lee[3,5], Bassam Estfan[9], Marc Shapiro[9], Suneel Kamath[9], Amr Mohamed[3,5], Stanley Ching-Cheng Huang[2,6], Alex Y. Huang[7], Ronald Conlon[1], Smitha Krishnamurthi[9], Jennifer Eads[3,5,10], Joseph E. Willis[6], Alok A. Khorana[9], David Bajor[3,5,*], Zhenghe Wang[1,2,*]

[1]Department of Genetics and Genome Sciences,
[2]Case Comprehensive Cancer Center,
[3]Department of Internal Medicine
[4]Department of Medical Genetics
[6]Department of Pathology
[7]Department of Pediatrics
[8]Department of Physiology and Biophysics
Case Western Reserve University,
10900 Euclid Avenue, Cleveland, Ohio 44106
[5]Seidman Cancer Center, University Hospitals Cleveland Medical Center, Cleveland, OH 44106
[9]Taussig Cancer Institute, Cleveland Clinic, Cleveland, Ohio 44195
[10]Department of Medicine, University of Pennsylvania, Philadelphia, PA 19104

***Corresponding authors**: Zhenghe Wang, BRB731, 10900 Euclid Avenue, Cleveland, Ohio 44106; Phone: 216-368-0446, Email: zxw22@case.edu;

David Bajor, 11100 Euclid Avenue Cleveland, OH 44106; Phone: (216) 286-4414, Email: david.bajor@uhhospitals.org

Conflict of Interest: The authors declare no conflict of interest.

Abstract

Neutrophil Extracellular Traps (NETs), a web-like structure of cytosolic and granule proteins assembled on decondensed chromatin, kill pathogens and cause tissue damage in diseases. Whether NETs can kill cancer cells is unexplored. Here, we report that a combination of glutaminase inhibitor CB-839 and 5-FU inhibited the growth of *PIK3CA* mutant colorectal cancers (CRCs) in xenograft, syngeneic, and genetically engineered mouse models in part through NETs. Disruption of NETs by either DNase I treatment or depletion of neutrophils in CRCs attenuated the efficacy of the drug combination. Moreover, NETs were present in tumor biopsies from patients treated with the drug combination in a phase II clinical trial. Increased NET levels in tumors were associated with longer progression-free survival. Mechanistically, the drug combination induced the expression of IL-8 preferentially in *PIK3CA* mutant CRCs to attract neutrophils into the tumors. Further, the drug combination increased the levels of reactive oxygen species in neutrophils, thereby inducing NETs. Cathepsin G (CTSG), a serine protease localized in NETs, entered CRC cells through the RAGE cell surface protein. The internalized CTSG cleaved 14-3-3 proteins, released BAX, and triggered apoptosis in CRC cells. Thus, our studies illuminate a previously unrecognized mechanism by which chemotherapy-induced NETs kill cancer cells.

Introduction

Neutrophils are the most abundant leukocytes in peripheral blood and play a vital role in host defense against pathogens (1). Neutrophils kill pathogens, including bacteria and fungi, by phagocytosis and by releasing granular enzymes and reactive oxygen species (ROS) (1). It was first discovered in 2004 that neutrophils could trap and kill bacteria by releasing Neutrophil Extracellular Traps (NETs), which consist of decondensed chromatin, granular enzymes, and cytosolic proteins to form web-like structures (2). NETs release occurs primarily through a cell death pathway called netosis (1). In the netosis process, nuclear envelopes are dissembled, histones are citrullinated by protein-arginine deiminase 4 (PAD4), which leads to chromatin de-condensation, plasma membranes are ruptured, and NETs are released (3). Many proteins, including histone, myeloperoxidase (MPO), neutrophil elastase (NE), proteinase 3 (PR3), and Cathepsin G (CTSG), have been identified in NETs (4). It has been shown that NETs trap and kill bacteria, fungi, viruses, and parasites (3). NETs also cause tissue damage and are involved in autoimmune diseases, liver injury, and thrombosis (3). It remains unknown if NETs can kill tumor cells, although some studies suggest that NETs promote tumor progression and metastasis (5, 6).

PIK3CA, which encodes the p110α catalytic subunit of PI3 kinase (7), is frequently mutated in human cancers, including 30% of colorectal cancers (CRCs) (8). We found that *PIK3CA* oncogenic mutations render CRCs more dependent on glutamine (9). We further demonstrated that a combination of CB-839, a glutaminase inhibitor, and 5-FU induced *PIK3CA* mutant CRC regression in multiple xenograft models in nude mice (10). These results prompted clinical trials testing the drug combination in human CRC patients (10). Here, we report a surprising finding that

the combination of CB-839 and 5-FU induces NETs, which release serine protease CTSG, in *PIK3CA* mutant tumors. CTSG enters CRC cells through cell surface protein RAGE, cleaves 14-3-3ε, causes BAX mitochondrial translocation, and induces apoptosis. Moreover, we conducted a phase II clinical trial of a combination of CB-839 and capecitabine, an oral prodrug of 5-FU, in metastatic *PIK3CA* mutant CRC patients who were refractory to prior fluoropyrimidine-based chemotherapy. The drug combination increases NETs in a majority of patients' tumors, which is associated with longer progression-free survival (PFS).

Results

Neutrophils modulate the anti-tumor effect of the combination of CB-839, a glutaminase inhibitor, and 5-FU.

Our previous study showed that the combination of CB839 and 5-FU treatment shrunk *PIK3CA* mutant CRC tumors in xenograft models in nude mice (10). To test if innate immunity could modulate the therapeutic effect of the drug combination, we simultaneously treated nude mice and NOD-SCID-gamma (NSG) bearing HCT116 CRC tumors, which harbor a *PIK3CA* mutation, with vehicle control, CB839, 5-FU, or the drug combination (Comb). Consistent with our previous results, the drug combination induced tumor regression in nude mice (Figure 1A). Surprisingly, the drug combination did not cause tumor regression in NSG mice (Figure 1B). The data suggest that innate immune cells modulate the tumor inhibitory effect of the drug combination.

To understand how innate immunity modulates the efficacy of the combination of CB-839 and 5-FU, we first tested if macrophages or NK cells played a role. However, neither the depletion of

macrophages nor NK cells impacted the tumor inhibitory effect of the drug combination in nude mice (Figure 1 C & D, Figure S1 A & B). Given neutrophils are recently reported to have anti-tumor effect (11), we next tested if a depletion of neutrophils had any impact on the anti-tumor effect of the combination of CB-839 and 5-FU. Indeed, the depletion of neutrophils using an anti-Ly6G antibody markedly blunted the tumor inhibitory effect of CB-839 plus 5-FU on HCT116 xenograft tumors (Figure 1 E, & Figure S1 C & D). Similarly, the depletion of neutrophils also attenuated the tumor inhibitory effect of the drug combination in DLD1 and RKO xenografts tumors (Figure 1 F & G). Together, our data suggest that neutrophils modulate anti-tumor effect of the drug combination.

However, both nude mice and NSG mice have functional neutrophils, which does not explain the observation that the anti-tumor effect of the combination of CB-839 and 5-FU was diminished in the NSG mice. Unlike in nude mice, we noted that NSG mice did not tolerate the drug combination well, and we had to give the mice two-day drug holidays after five-day drug treatment in NSG and nude mice, which resulted in the initial tumors growth at the beginning of the drug combination treatment in nude mice (Figure 1A). These results were different from nude mice treated with the daily drug combination that caused the continuous shrinkage of the tumors as we reported previously (10). Thus, we postulated that neutrophils in NSG mice might be more susceptible to the drug combination. We treated nude mice and NSG mice with either vehicle or the combination of CB-839 and 5-FU for seven days and counted circulating blood cells in these mice without tumors implanted. As shown in Figure S1E, compared to vehicle treatment, the relative number of

neutrophils substantially decreased in NSG mice treated with the drug combination, whereas the drug combination did not impact neutrophils in nude mice.

Neutrophil extracellular traps (NETs) module the anti-tumor effect of the combination of CB-839 and 5-FU.

Given that two previous studies suggested that NETs could suppress tumor growth in vitro (11, 12), we thus stained the tumors harvested from the experiments shown in Figure 1 A & B with antibodies against citrullinated histone H3 (H3cit) that marks NETs, and myeloperoxidase (MPO) that marks both NETs and neutrophils (5). Interestingly, the drug combination induced NETs in tumors in nude mice but not in NSG mice quantified using two different formulas (Figure 1 H-L, and Figure S1 F -I). Moreover, tumors in nude mice treated with the drug combination had substantially more neutrophils than tumors treated with vehicle (Figure 1I & Figure S1F). In contrast, tumors in NSG mice did not have many infiltrating neutrophils (Figure 1K & Figure S1H). Similar results were observed in DLD1 and RKO xenograft tumors in nude mice (Figure 1 M to P, & Figure S1 J-M). However, the drug treatment had no impact on tumor-infiltrating macrophages and NK cells (Figure S1 N-P).

To determine if NETs induced by the CB-839 plus 5-FU treatment inhibit tumor growth, we set out to deplete NETs using DNase I treatment. We injected HCT116 CRC cells subcutaneously into nude mice. Once tumors reached an average size of 200 mm^3, mice were randomly assigned to four groups and treated by vehicle, vehicle + DNase I, CB-839 + 5-FU, and CB-839 + 5-FU +

DNase I. As shown in Figure 2A, DNase I treatment substantially attenuated the tumor inhibitory effect of the combination of CB-839 and 5-FU, whereas DNase I treatment did not impact the growth of tumors treated with vehicle. Immunofluorescence staining of the tumors showed that DNase I drastically reduced levels of H3cit (a NET marker), but did not impact MPO levels (a neutrophil marker) in tumors treated with the combination of CB-839 and 5-FU (Figure 2 B & C, and Figure S2A). Similarly, DNase I treatment disrupted NETs and attenuated the tumor inhibitory effect of the combination of CB-839 and 5-FU in DLD1 and RKO xenografts tumors (Figure 2 D to G, and Figure S2 B & C), Moreover, a neutrophil elastase inhibitor sivelestat, which was shown to block NETs formation (13), also attenuated the anti-tumor effect of the drug combination (Figure S2D) and reduced the levels of H3cit in the tumors (Figure S2E). Consistently, the depletion of neutrophils drastically reduced levels of both H3cit and MPO in tumors treated with CB-839 plus 5-FU (Figure S2 F-L). Together, these data suggest that NETs modulate the anti-tumor effect of the drug combination.

The combination of CB-839 and 5-FU upregulates IL-8 in *PI3KCA* mutant tumors to recruit neutrophils.

We next set out to determine how the combination of CB-839 and 5-FU induces NETs. We first performed RNA-seq on isogenic DLD1 *PIK3CA* WT-only and Mut-only cell lines (14) treated with either vehicle or the combination of CB-839 and 5-FU, because the drug combination induced more NETs and tumor-infiltrating neutrophils in *PIK3CA* Mut-only tumors than the isogenic WT-only tumors (Figure S3 A & B). Over 125 genes were differentially expressed in *PIK3CA* Mut-only cells upon the combinational drug treatment (Figure S3 C & D, Table S1). Pathway analyses

revealed that the inflammatory response pathway, which includes the neutrophil chemokine IL-8, was one of the most significantly enriched pathways (Figure S3E). Second, we profiled cytokines in the isogenic DLD1 *PIK3CA* WT-only and Mut-only cell lines. Again, the drug combination induced more IL-8 in *PIK3CA* Mut-only cells than in the isogenic *PIK3CA* WT-only cells (Figure S4F). Other neutrophil chemokines, including CXCL1, CXCL2, and CXCL5, were not upregulated by the drug treatment (Figure S3G). Moreover, the drug combination induced IL-8 in parental HCT116, DLD1, and RKO cultured cells, as well as in xenograft tumors (Figure 3 A & B, and Figure S3H). It is worth noting that it has been demonstrated by many studies that human IL-8 can act as chemokine to attract mouse neutrophils (15-20).

To test if the drug combination-induced IL-8 attracts neutrophils and modulates the tumor-inhibitory effect, we knocked out IL-8 in three different CRC cell lines, including HCT116, DLD1, and RKO (Figure S3 I & J). Two independently derived *CXCL8*/*IL-8* knockout (KO) clones from each cell line were used for in-depth analyses. As shown in Figure 3 C to E, *IL-8* knockout attenuated the tumor-inhibitory effect of the combination of CB-839 and 5-FU and reduced tumor-infiltrating neutrophils and NETs in HCT116 xenograft tumors. Similar results were observed with *IL-8* KO DLD1 and RKO cells (Figure 3 F to I). As a control, we knocked out *CXCL1* in HCT116 cells (Figure S3 K & L), which did not impact the xenograft tumor growth (Figure S3M). The *CXCL1* KO did not attenuate the anti-tumor effect of the drug combination (Figure S3M). Moreover, to test if a gene knockout that leads to reduced tumor growth would impact the anti-tumor effect of the drug combination, we chose to treat *ERBB3* knockout tumors, which resulted in reduced xenograft tumor growth (21). As shown (Figure S3 N & O), knockout of ERBB3 did

not attenuate the anti-tumor effect of the drug combination. Together, these results suggest that the combination of CB-839 and 5-FU induced IL-8 expression in cancer cells, which attracts neutrophils to form NETs and augments the anti-tumor effect of the drug combination.

The combination of CB-839 and 5-FU activates NRF2 to induce *IL-8* gene transcription.

We next interrogated how IL-8 was induced by the combination of CB-839 and 5-FU in CRC cells. qRT-PCR analyses showed that IL-8 mRNA expression was substantially up-regulated in HCT116, DLD1, and RKO CRC cells by the drug combination (Figure 3A). It was reported that NRF2 is a transcription factor for IL-8 (22). We have demonstrated that the combination of CB-839 and 5-FU induces reactive oxygen species (ROS) and activates NRF2 transcriptional activity preferentially in *PIK3CA* mutant CRCs compared to isogenic *PIK3CA* WT CRCs (10). Thus, we knocked down NRF2 in HCT116, DLD1, and RKO with two independent siRNA (Figure S3P). Figure 3 J & K showed that the knockdown of NRF2 substantially reduced NRF2 mRNA and protein expression induced by the combination of CB-839 and 5-FU in HCT116, DLD1, and RKO cells. To further validate these results, we knocked out *NRF2* in HCT116 and DLD1 cells (Figure S3 Q & R). Consistent with the siRNA knockdown results, the knockout of *NRF2* substantially reduced the drug-induced IL-8 expression (Figure S3S). We failed to obtain any *NRF2* KO clones in RKO cells, suggesting that NRF2 may be an essential gene for RKO. There are six putative NRF2 binding sites in the promoter region of the *IL-8* gene. ChIP-qPCR analyses indicated the drug combination induced NRF2 binding to three of them (Figure S3T). Together, the data suggest that the combination of CB-839 and 5-FU activates NRF2 transcriptional activity in CRC cells and

induces IL-8 expression, thereby attracting neutrophils into tumors and producing NETs to inhibit tumor xenograft tumor growth.

The combination of CB-839 and 5-FU increases reactive oxygen species (ROS) levels in neutrophils to induce NETs.

To determine how the combination of CB-839 and 5-FU induces NETs, we isolated and purified neutrophils from the bone marrow of C57/BL6 mice (Figure S4A) and treated them with DMSO, CB-839, 5-FU, or the drug combination. Neutrophils were treated with PMA in parallel as a positive control. As shown in Figure 4 A & B & S4 B to D, CB-839 induced a small number of NETs (fiber-like DNA coated with citrullinated H3 and MPO), whereas 5-FU induced a nominal number of NETs. However, the drug combination induced many web-like NETs with long DNA fibers (Figure 4 A & B & Figure S4 B to D). Interestingly, the PMA treatment induced a large amount of H3cit (Figure 4A). However, NETs induced by PMA lack long DNA fibers (Figure S4D). The drug-induced NET formation is dependent on PAD4, because the PAD4 inhibitor GSK484 blocked the NET formation induced by the drug combination (Figure S4E).

It was reported that IL-8 could induce NETs (23). Given that we have shown that the drug combination induces IL-8 expression in CRC cells, we then treated the purified neutrophils with various amounts of IL-8. However, IL-8 failed to induce NETs in this setting (Figure S4 F & G), which is consistent previous reports (24, 25).

It is well-documented that ROS induces NET in neutrophils. Given that we reported previously that the combination of CB-839 and 5-FU induces ROS (10), we set out to determine if the drug combination induces NETs through ROS production. Indeed, the combination of CB-839 and 5-FU substantially increased ROS levels in neutrophils (Figure 4C), although it was a weaker ROS inducer than PMA. Nonetheless, ROS scavenger diphenyleneiodonium (DPI) reduced ROS levels in neutrophils and amounts of NETs induced by the drug combination (Figure 4C). Together, the in vitro data suggest that the combination of CB-839 and 5-FU induces NETs through ROS production in neutrophils. However, we cannot rule out the possibility that ROS acts in concert with other factors generated by the drug combination to produce NETs.

To interrogate how NETs inhibit CRCs, we treated neutrophils with the combination of CB-839 and 5-FU to induce NETs, and conditioned medium (NET medium) from this culture was transferred to a new well which contains HCT116 CRC cells (Figure 4D). Compared to cells grown in a normal medium or conditioned medium from HCT116 cells treated with the drug combination, the NET medium inhibited HCT116 cell growth and induced apoptosis in a dose-dependent manner (Figure 4E-4I). Although we reported previously high doses of CB-839 (20 μM) and 5-FU (10 μM) combination induced apoptosis of HCT116 cells, the low doses of CB-839 (1 μM) and 5-FU (1 μM) we used here for NET induction did not increase apoptosis compared to controls (Figure S4H). Moreover, conditioned media from neutrophils without drug treatment or treated with a neutrophil activator N-Formylmethionyl-leucyl-phenylalanine (fMLP) did not induce apoptosis in HCT116 cells (Figure S4I). Consistently, the combination of CB-839 and 5-FU

treatment substantially increased apoptosis in HCT116, DLD1, and RKO xenograft tumors in nude mice (Figure 4 J & K, Figure S4 J & K). We have shown that either DNase I treatment or neutrophil depletion attenuated the anti-tumor effect of the drug combination. Consistent with these results, DNase I treatment or neutrophil depletion substantially reduced apoptosis induced by the drug combination in xenograft tumors (Figure 4L-O, Figure S4 L & M). The data suggest that components in NETs may kill CRC cells by inducing apoptosis.

We next treated neutrophils with various chemotherapy drugs to test if other cancer drugs could induce NETs. Figure S4 N & O show that camptothecin gemcitabine, daunorubicin, epirubicin, and regorafenib also induced NETs, suggesting that NET induction may be a mechanism by which some chemotherapies inhibit tumor growth.

Cathepsin G in NETs kills cancer cells.

Neutrophil extracellular traps (NETs) consist of web-like DNA and associated granular proteins (1). To test if any of the proteins in NETs could induce apoptosis of CRC cells, we treated HCT116 cells with recombinant LL-37, neutrophil elastase (NE), protein 3 (PR-3), cathepsin G (CTSG), or lactoferrin (LF). As shown in Figure 5 A to G and Figure S5A, only CTSG, a serine protease, inhibited HCT116 cell growth and induced apoptosis in a dose-dependent manner. Interestingly, the NET medium contains CTSG (Figure S5B). In contrast, conditioned media of neutrophils treated with either fMLP or PMA had a nominal amount of CTSG, which explains that conditioned media from both treatments did not induce much apoptosis (Figure S4I & Figure S5 B-D). These

data suggest that NETs induced by the combination of CB-839 and 5-FU may be distinct from NETs induced by PMA. Consistently, NETs induced by the drug combination had more DNA fibers than NETs induced by PMA (Figure S4D). Moreover, a non-cell permeable cathepsin G inhibitor I (CTSGi) (26), which potently inhibits CTSG protease activity, attenuated apoptosis induced by either recombinant CTSG or conditioned medium from neutrophils treated with CB-839 and 5-FU (NET medium) in a dose-dependent manner (Figure S5 E-K) in HCT116, DLD1, and RKO CRC cells. In contrast, an NE inhibitor sivelestat only marginally inhibited apoptosis of colon cancer cells treated with NET conditioned medium (Figure S5 L & M). The marginal effect of sivelestat may be due to its low activity in inhibiting CTSG (27). Together, those data suggest that cathepsin G released from NETs kills CRC cells.

To test if CTSG plays a critical role in the tumor inhibitory effect of the combination of CB-839 and 5-FU mediated by NETs in vivo, we treated HCT116 xenograft tumors established subcutaneously in nude mice with vehicle control or the drug combination with or without CTSGi. As shown in Figure 5H, the cathepsin G inhibitor substantially attenuated the tumor inhibitory effect of CB-839 and 5-FU, whereas the inhibitor had no impact on tumors treated with vehicle. Consistently, CTSGi treatment reduced apoptosis in tumors treated with the drug combination (Figure 5 K & L). Similar results were observed with RKO and DLD1 xenograft tumors (Figure 5 I & J, M & N). Moreover, the CTSGi did not reduce levels of NETs induced by the combinational drug treatment (Figure 5 O to Q, Figure S5 N to T). Given that we have shown that DNase I treatment attenuated the anti-tumor effect of the drug combination (Figure 2A), we postulated that the decondensed DNAs in NETs anchor CTSG within tumors, without which CTSG proteins could

be washed out. In support, the western blot analyses showed that the drug combination induced CTSG protein levels were reduced in tumors treated with DNase I (Figure S5 U & V).

CTSG enters cancer cells through RAGE.

To test if CTSG can enter CRC cells to trigger apoptosis, we incubated recombinant CTSG with HCT116 cells. Immunofluorescent staining showed that CTSG was on the cell surface 15 minutes after CTSG was added (Figure 6A) and predominantly inside cells after 4 hours (Figure 6A). Given that CCDC25 is reported to be a receptor for NET DNAs (28), we tested whether CTSG enters cancer cells through CCDC25-mediated NET DNA-CTSG complex internalization. We knocked out *CCDC25* in HCT116 and DLD1 cells using CRISPR/Cas 9-mediated genome editing (Figure S6A). However, the knockout of *CCDC25* did not impair the entrance of CTSG into cancer cells (Figure S6B). Moreover, the knockout of *CCDC25* did not affect CTSG-induced apoptosis in both HCT116 and DLD1 cells (Figure S6C), nor did it impact the anti-tumor effect of the drug combination (Figure S6D). These results suggest that the NET DNA-CCDC25 pathway is not involved in the CTSG-induced apoptosis of CRC cells. We next turned our attention to cell surface protein RAGE, because it was shown that RAGE mediated neutrophil-derived CTSG cytotoxicity (29). We knocked out *RAGE* in HCT116, DLD1, and RKO CRC cells using CRISPR/Cas 9-mediated genome editing (Figure S6F). Indeed, the knockout of *RAGE* blocked the entrance of CTSG into HCT116, DLD1, and RKO cells (Figure 6A and Figure S6G). Moreover, knockout of *RAGE* abrogated apoptosis induced by CTSG or NET medium in HCT116, DLD1, and RKO cells (Figure 6B and Figure S6H). In contrast, PR3 did not enter any of the CRC cells (Figure S6I). NE

failed to enter HCT116 and RKO CRC cells, although it entered DLD1 cells (Figure S6I). However, *RAGE* KO did not prevent NE from entering DLD1 cells.

Next, we tested if the knockout of *RAGE* attenuates the tumor-inhibitory effect of the combination of CB-839 and 5-FU. As shown in Figure 6 C to E, the drug combination did not induce tumor regression of *RAGE* knockout HCT116, DLD1, and RKO CRCs. Consistently, *RAGE* knockout attenuated the drug combination-induced apoptosis in tumors (Figure 6 G-J). Together, the data suggest that RAGE mediates the entrance of CTSG into CRC cells.

CTSG cleaves 14-3-3ε, induces BAX mitochondrial translocation, and triggers apoptosis.

Given that CTSG is a serine protease, we postulated that CTSG might cleave an anti-apoptotic protein to trigger apoptosis. However, neither BCL2 nor VDAC was cleaved when HCT116 cells were incubated with recombinant CTSG (Figure S7A). We then turned our attention to 14-3-3 proteins because it was predicted to be a substrate of CTSG. Moreover, 14-3-3 proteins were shown to bind and sequester BAX from mitochondria, thereby preventing apoptosis (30). Indeed, 14-3-3ε protein levels were decreased when HCT116 cells were incubated with recombinant CTSG (Figure 6F). In contrast, CTSG had either no or marginal effect on other 14-3-3 isoforms (Figure S7A). Moreover, 14-3-3ε protein levels were decreased when CRC cells were incubated with NET medium (Figure 6F and Figure S7A). We then tested if CTSG could cleave 14-3-3ε in vitro. As shown in Figure S7B, CTSG cleaves 14-3-3ε in a time-dependent manner. Similarly, 14-3-3ε can be cleaved by incubating with NET medium, and this cleavage could be suppressed by

CTSGi (Figure S7C), but not DNase I (Figure S7D). Furthermore, compared to vehicle controls, 14-3-3ε protein levels were also decreased in HCT116 xenograft tumors treated with the combination of CB-839 and 5-FU (Figure 6 K and Figure S7E). Consistent with the notion that the drug combination induces NETs, the combination of CB-839 and 5-FU treatment induced higher levels of citrullinated H3 (H3-cit) and MPO in the HCT116 xenograft tumors (Figure 6 K and Figure S7E). Similar results were observed with DLD1, RKO cells, and their xenografts (Figure 6 L & M, Figure S7 F & G). Together, these data suggest that CTSG enters CRC cells, cleaves 14-3-3ε, and triggers apoptosis.

Given that 14-3-3 binds to BAX and sequesters it from mitochondria to prevent apoptosis (30), we examined if CTSG treatment resulted in BAX mitochondrial translocation. As shown in Figure 6 N to P, CTSG treatment led to BAX mitochondrial translocation in HCT116, DLD1, and RKO) cells. Consistently, cytochrome c was released from the mitochondria to the cytosol (Figure 6 N to P, & Figure S7 H to J). Similarly, treating HCT116 cells with NET medium also induced BAX mitochondrial translocation (Figure S7K), and this process could be suppressed by CTSGi (Figure S7L). Together, our data suggest that CTSG enters CRC cells, cleaves 14-3-3ε, causes BAX mitochondrial translocation, and triggers apoptosis.

NETs modulate the anti-tumor effort of the combination of CB-839 and 5-FU in *PIK3CA* mutant mouse colon tumors in immune-competent mice.

To test if the drug combination induces NETs in immune-competent mouse tumor models, we generated *Pik3ca* E545K oncogenic mutant knockin CMT93 and MC38 mouse colon cancer cell

lines using CRISPR-mediated genome editing (Figure S8 A & B). We then injected parental or *Pik3ca* mutant cells subcutaneously into immune-competent C57/BL6 mice and treated them with the vehicle, CB-839, 5-FU, or the drug combination. As with human CRCs, the drug combination induced tumor regression and apoptosis of *Pik3ca* mutant, but not parental, CMT93 tumors (Figure 7 A & B, Figure S8 C & D). Moreover, the combination of CB-839 and 5-FU induced NETs in *Pik3ca* mutant, but not parental, CMT93 tumors (Figure 7 C to E, Figure S8 F & G). A single drug alone did not induce NETs in any of the tumors (Figure 7 C to E). Similar results were observed with *Pik3ca* mutant MC38 mouse colon tumors (Figure 7 F to J, Figure S8 E, H & I). In contrast to the xenograft models with human CRC cell lines, the drug combination did not induce more tumor-infiltrating neutrophils compared to vehicle or single drugs (Figure 7 D & I). However, the *Pik3ca* mutant tumors had more tumor-infiltrating neutrophils than tumors of the parental counterparts (Figure 7 C & D, 7 H & I).

PIK3CA mutations in human cancers occur in two hotspots: one in the helical domain (e. g. E545K) and the other in the kinase domain (H1047R). We have successfully constructed a *CDX2P-CreER*^{T2} *Apc*$^{flox/+}$ *Kras*$^{LSL\text{-}G12D/+}$ *Pik3ca*$^{LSL\text{-}H1047R/+}$ mouse (GEM) model (31), in which an allele of Apc is inactivated, and Kras G12D and *Pik3ca* H1047R oncogenic mutations are activated by colon-specific and inducible CDX2P-CreER^{T2} transgene upon tamoxifen treatment. Mice were treated with vehicle, CB-839, 5-FU, or the drug combination for three weeks. As shown in Figure 7K, the drug combination, but not a single drug alone, substantially extended the survival of the mice. Consistently, the drug combination, but not a single drug, induced NETs (Figure 7 L-N, Figure S8 J & K). As with the syngeneic models, the drug treatments did not induce more tumor-infiltrating neutrophils compared to vehicle treatment (Figure 7 L & M, Figure S8J). Together, the

data demonstrate that the combination of CB-839 and 5-FU induces NETs in *Pik3ca* mutant tumors in syngeneic and GEM immune-competent mouse models.

As with the xenograft models, DNase I treatment, which disrupted NET formation, attenuated the anti-tumor effect of the combination of CB-839 and 5-FU in CMT93 and MC38 *Pik3ca* E545K mutant syngeneic mouse models (Figure 8 A & B). Notably, DNase I treatment reduced the levels of NETs (Figure 8 E & G, J & L), but did not impact the numbers of tumor-infiltrating neutrophil (Figure 8 C-L). Together, our data provide further evidence that NETs modulate the anti-tumor effect of the combination of CB-839 and 5-FU.

CXCL5, a neutrophil chemokine, is upregulated in *Pik3ca* mutant mouse colon cancer cells through the NF-κB pathway.

Because the mouse does not have an IL-8 homolog (32), we next investigated what chemokine(s) attracted neutrophils to tumors in the mouse syngeneic models. Given that CXCL1, CXCL2, and CXCL5 are the known neutrophil chemokines in mice (33), we measured mRNA expression of these chemokines in CMT93 parent and *Pik3ca* E545K KI cells treated with vehicle or the combination of CB-839 and 5-FU. As shown in Figure 9 A to C, CXCL5 expression levels were upregulated in *Pik3ca* mutant CMT93 cells compared to the parental counterparts, regardless of the drug treatment. In contrast, there was no difference in CXCL1 levels among the different conditions (Figure 9A), whereas CXCL2 mRNA levels decreased in *Pik3ca* E545K KI CMT93 cells compared to the parental cells (Figure 9B). It is worth noting that CXCL1 and CXCL2 were expressed at much lower levels than CXCL5 (Figure 9C). Similarly, CXCL5 upregulated in MC38

Pik3ca E545K KI cells compared to parental cells (Figure 9 D & E). Thus, we focused on CXCL5 for in-depth studies. ELISA analyses showed that secreted CXCL5 proteins were upregulated in *Pik3ca* mutant CMT93 and MC38 tissue cultured cells and syngeneic tumors (Figure 9 F to I). Notably, CXCL5 is not regulated by mutant *PIK3CA*/p110α in human CRC cells (Figure S3G). We postulate that the promoters of CXCL5 in mouse and human are different and therefore have different responses to *PIK3CA*/p110α mutation.

We next set out to identify the mechanisms by which the *Pik3ca* mutation up-regulates CXCL5. It was reported that NF-κB regulates CXCL5 transcriptionally (34) and that *PIK3CA* mutations activate the NF-κB pathway (35). We thus knocked down p65 with two independent siRNA in *Pik3ca* E545K mutant CMT93 and MC38 cells. Figure 9 J to O show that the knockdown of p65 resulted in decreased levels of CXCL5 mRNA and secreted proteins. ChIP-qPCR analyses showed that p65 bound to the promoter regions of CXCL5 in *Pik3ca* E545K mutant CMT93 cells (Figure 9P). Together, the data suggest that *Pik3ca* mutation activates the NF-κB pathway to upregulate CXCL5 in mouse CRCs, thereby attracting more tumor-infiltrating neutrophils.

CTSG plays a key role in anti-tumor effect of the combination of CB-839 and 5-FU in syngeneic models.

Given that we have demonstrated in xenograft models that CTSG in the NETs plays a key role in killing cancer cells, we set to determine whether the same is true for the syngeneic models. We first tested if the CTSG inhibitor (CTSGi) could attenuate the anti-tumor effect of the combination. As shown in Figure 10 A to E and Figure S9 A & B, CTSGi treatment indeed attenuated the

therapeutic effect and apoptosis induced by the drug combination in both CMT93 and MC38 *Pik3ca* E545K mutant tumor models. As with the xenograft models, CTSGi treatment did not perturb NET formation (Figure 10 F to J, Figure S9 C & D).

To test rigorously if CTSG is required for the tumor inhibitory effect of the combination of CB-839 and 5-FU, we obtained a *Ctsg* knockout C57/Bl6 mouse strain. Western blot analyses validated the knockout of CTSG (Figure S9E). We then injected MC38 *Pik3ca* E545K mutant cells into $Ctsg^{-/-}$ mice and their $Ctsg^{+/+}$ littermates. Once tumors reached an average size of 100 mm^3, mice were treated with vehicle or a combination of CB-839 and 5-FU. As shown in Figure 10 K to M, the tumor inhibitory effect and apoptosis induced by the drug combination was attenuated in $Ctsg^{-/-}$ mice compared to their WT littermates. Surprisingly, although the number of tumor-infiltrating neutrophils was not decreased in $Ctsg^{-/-}$ mice (Figure 10 N & O, Figure S9F), the levels of NETs induced by the drug combination were substantially reduced in syngeneic tumors in $Ctsg^{-/-}$ mice compared to the $Ctsg^{+/+}$ littermates (Figure 10P, Figure S9G). We then isolated neutrophils from $Ctsg^{+/+}$ and $Ctsg^{-/-}$ mice and treated them with vehicle or the combination of CB-839 and 5-FU. Figure S9 H & I show that the drug combination failed to induce NETs in vitro, suggesting that CTSG is involved in NET induction in neutrophils by the drug combination. Notably, a previous study suggested that CTSG was involved in NET formation as well (36). Consistently, the conditioned medium of neutrophils from $Ctsg^{-/-}$ mice treated with CB-839 and 5-FU reduced apoptosis induction in CRC cells (Figure S9J). It is worth noting that the CTSG inhibitor (CTSGi) that we used in the experiments described in Figure 5 H to J and Figure 10 A to E is not cell permeable. Thus, it only inhibits CTSG in the NETs, not CTSG inside neutrophils, thereby not

preventing NETs induction as shown in Figure S5 N to T and Figure 10 H & J. Together, our results suggest that CTSG plays a critical role in modulating the tumor-inhibitory effect of the drug combination.

Lastly, we have shown that CTSG enters human CRC cells to cleave 14-3-3ε to trigger apoptosis. We set out to test if the same mechanism occurred in mouse colon cancer cells. As shown in Figure 10Q, treating CMT93 and MC38 *Pik3ca* mutant cells with either recombinant CTSG or NET-conditioned medium resulted in dramatically reduced levels of 14-3-3ε. As with the xenograft models, the combination of CB-839 and 5-FU decreased the levels of 14-3-3ε in the syngeneic CMT93 and MC38 *Pik3ca* E545K mutant tumor models (Figure 10 R & S).

A phase II clinical trial of a combination of CB-839 with capecitabine, an oral prodrug of 5-FU, in metastatic *PIK3CA* mutant CRC patients.

We previously conducted a phase I clinical trial of the combination of CB-839 and capecitabine in advanced solid tumor patients and showed that the drug combination was well tolerated (10). The recommended phase II dose (RP2D) was CB-839 800 mg by mouth twice daily continuously and capecitabine 1,000 mg/m^2 orally twice daily on days 1-14 of a 21-day treatment cycle (10). In this trial, we observed ~40% of patients with *PIK3CA* mutated metastatic CRC had over six months of progression-free survival (PFS). Here, we conducted a phase II clinical trial on metastatic *PIK3CA* mutant CRC patients who were refractory to prior fluoropyrimidine-based chemotherapy. The primary objective was assessing PFS greater than six months. Thirty-two eligible patients, whose ages ranged from 37 to 81 years old, with a median age of 56, were treated with the drug

combination. The baseline patient characteristics are shown in Table S2, and the PFS of these patients are shown in Figure 11A. The median PFS of the patients is 75 days (range 36 to 251 days), and seven patients had over 6-month PFS (21.8%). Of 28 patients who were evaluable for response, 14 patients (50%) had stable disease, and 14 had progressive disease as the best response. Although no objective response was observed, five patients had tumor regression (range 1% to 15% reduction of overall tumor burden). The combination was again adequately tolerated (Table S3), with a toxicity profile similar to what we observed in the phase I clinical trial patients (10).

Increased levels of NETs in posttreatment tumor biopsies are associated with longer PFS.

Of the 32 patients, we obtained pre- and posttreatment biopsy pairs in 24 patients. We stained the 24 biopsy pairs with antibodies against MPO and citrullinated H3. Compared to pretreatment counterparts, MPO levels were increased in the posttreatment biopsies of 17 patients, decreased in 5 patients, and were not changed in 2 patients (Figure 11 B & C). The levels of citrullinated H3 were increased in the posttreatment biopsies in 15 patients, decreased in 1 patient, and not changed in 8 patients (Figure 11 B & C). In 14 patients, both MPO and citrullinated H3 levels increased in posttreatment biopsies, suggesting that the combinational treatment of CB-839 and capecitabine led to increased tumor-infiltrating neutrophils and induction of NETs. In one patient, the levels of citrullinated H3 increased in posttreatment biopsy without a change in MPO levels. Interestingly, patients who had increased levels of citrullinated H3 (marking NETs) in posttreatment biopsies over pretreatment biopsies were associated with long PFS (Figure11D). Moreover, when taking account citrullinated H3 levels only in posttreatment biopsies, higher levels of citrullinated H3

were also associated with longer PFS (Figure 11E). However, the increased levels of tumor-infiltrating neutrophils (MPO positive cells) were not associated with long PFS (Figure S10B).

Discussion

We reveal here a previously unrecognized mechanism by which chemotherapy inhibits tumor growth. Our studies demonstrated that the combination of CB-839 and 5-FU induces NETs to inhibit in vivo growth of tumors with a *PIK3CA* mutation in xenograft, syngeneic, and GEM models. Furthermore, disruption of NETs by DNase I treatment or depletion of neutrophils attenuates the tumor-inhibitory effect of the drug combination. In the phase II clinical trial, the drug combination induces NETs in tumors in most patients, and the increased levels of NETs are associated with longer PFS. NETs were first identified as a mechanism by which neutrophils trap and kill bacteria (2). Follow-up studies show that NETs also kill fungi and parasites. Recent studies also demonstrate that NETs cause tissue damage in a variety of pathologic conditions, including autoimmune diseases (37), thrombosis (38), liver injury (39), and toxic epidermal necrolysis (40). However, to the best of our knowledge, it has not been reported so far that induction of NETs in vivo by any anti-cancer drugs inhibits tumor growth. Moreover, in addition to the combination of CB-839 and 5-FU, our data showed that six other chemotherapy drugs could also induce NETs in vitro, suggesting that induction of NETs may be an unappreciated mechanism by which some chemotherapies inhibit tumor growth. It is worth noting that recent studies demonstrated that spontaneous NETs, which occur at low levels, promote tumor metastasis by extracellular matrix remodeling (5). In contrast, the combination of CB-839 and 5-FU induces a large number of NETs that kill cancer cells through the action of protease cathepsin G. Nonetheless, it has been shown

that NETs play a role in radiotherapy resistance (41). Moreover, a recent study showed that chemotherapy induces cancer cells to release IL-1β to promote NET formation, which in turn activates latent TGFβ secreted by cancer cells and causes chemoresistance (42).

Mechanistically, we demonstrated here that the combination of CB-839 and 5-FU induces IL-8 expression in *PIK3CA* mutant CRC cells, thereby attracting neutrophils into the tumor tissues. On the other hand, the drug combination acts on neutrophils to induce NETs and release CTSG. CTSG enters cancer cells through cell surface protein RAGE and cleaves 14-3-3ε, which leads to BAX mitochondrial translocation and triggers apoptosis of cancer cells (Figure 11F). Here, we provide several pieces of evidence to support such mechanisms: 1) knockout of *IL-8* in CRC cells attenuates the tumor inhibitory effect of the combination of CB-839 and 5-FU; 2) a non-cell-permeable CTSG inhibitor, which does not perturb NET induction, attenuates the tumor inhibitory effect of the drug combination; 3) the drug combination is less effective on syngeneic *Pik3ca* mutant tumors in *Ctsg* knockout mice compared to the WT littermates, although the drug combination induces fewer NETs in tumor in the *Ctsg* knockout mice, suggesting that CTSG may be involved NET induction process in neutrophils; 4) knockout of *RAGE* attenuates the tumor inhibitory effort of the drug combination; 5) CTSG treatment reduces 14-3-3ε levels in cultured CRC cells and cleaves recombinant 14-3-3ε in vitro; 6) the combination of CB-839 and 5-FU reduces 14-3-3ε levels in xenograft and syngeneic tumors; and 7) CTSG treatment induces BAX mitochondrial translocation in cultured CRC cells. As mentioned above, NETs have been shown to be involved in many pathogenic conditions that cause tissue damage. However, the detailed mechanisms by which NETs damage tissues in these conditions remain elusive. We postulated that

the mechanisms we uncovered here might be applicable to other pathogenic conditions, which warrants further investigation.

The phase II clinical trial of CB-839 and capecitabine in patients with *PIK3CA*-mutated colon cancer reported here had 21.8% patients surpassing six months PFS, which did not meet its pre-specified objective of 25% of patients with over six months PFS. Although five patients had reduced overall tumor burden, no patient had a reduction greater than 30%. Nonetheless, the currently demonstrated immune mechanism could inform future clinical trial designs. Potential future studies should ensure adequate circulating neutrophil counts throughout treatment cycles as diminished neutrophils abrogate the effectiveness of the combination in animal models (Figure S1E). We note that G-CSF is a clinically available agent that is typically administered to reduce infection risk in patients receiving myeloablative or highly myelosuppressive chemotherapy regimens (43), but not to patients receiving capecitabine. Thus, these findings may now serve as a basis for future trials in which the use of G-CSF is tested in combination with agents such as CB-839 and capecitabine, to ensure that the potential anti-tumor benefit of neutrophils is maximized during the treatment course. In support, patients who had longitudinally increased neutrophil numbers post-drug treatment had longer PFS than those who had decreased neutrophil numbers after the drug treatment in the phase II clinical trial (Figure S10C). Notably, these data are different from the tumor-infiltrating neutrophils on day 10 to 14 biopsies, which represented a short-term snapshot and had no predictive value for PFS (Figure S10B). We postulate that the long-term effect of the drug treatment on neutrophils and NET formation in tumors may have better predictive value. More generally, these findings may serve as a basis for preclinical and clinical exploration

of a potential therapeutic advantage for maximizing neutrophils in therapies with other traditional cytotoxic anti-cancer drugs. Moreover, we showed here that increased NET levels post-drug treatment are associated with longer PFS (Figure 11 D & E). Given that a recent study showed that PD-L1 modulates NET induction (44), further studies combining NET-inducing treatments such as this with checkpoint inhibition to harness adaptive immune mechanisms may also be warranted.

Methods

All reagents used in this study are listed in Table S4.

Mouse experiments

Our examined both male and female animals. Similar findings are reported in both sexes.

For HCT116, DLD1, and RKO human colon cancer cell lines, 2×10^6 cells were injected subcutaneously and bilaterally into 6-week-old nude or NSG mice as described previously (45). For CMT93 and MC38 cells, 5×10^6 of WT or *PIK3CA* E545K mutant knock-in cells were injected subcutaneously and bilaterally into the flanks of 6-week-old C57BL/6 mice (Jackson Lab, ME). Once tumors reached an average volume of 150 mm^3, mice were randomly divided into different treatment groups. Mice were treated daily with vehicle control, CB839 (200 mg/kg, oral gavage, provided by Calithera Biosciences), 5-FU (30 mg/kg, i.p.), or the drug combination. For neutrophil elastase inhibitor treatment, mice were treated daily with vehicle control or sivelestat (10 mg/kg) by intraperitoneal (IP) injection. Tumor volume was measured with calipers, and volumes were calculated as length × $width^2/2$.

For the CDX2P-CreER^{T2} *Apc*$^{flox/+}$ *Kras*$^{LSL\text{-}G12D/+}$ *Pik3ca*$^{LSL\text{-}H1047R/+}$ mouse (GEM) model, 8-week-old mice were injected intraperitoneally with tamoxifen (100 mg/kg, dissolved in corn oil) for three consecutive days. For survival analysis, mice were randomly assigned into four treatment groups a week after tamoxifen injection and treated with vehicle control, CB839, 5-FU, or the drug combination for 4 weeks. For netosis staining, mice were treated with the drugs for 27 days after the tamoxifen injection for a week. Colon tumor tissues will be fixed and stained with netosis markers for further analysis.

Phase II clinical trial design

Both male and female patient are enrolled for the studies. This clinical trial was conducted with the approval of the institutional review board and according to good clinical practice with a primary objective of determining the rate of 6-month progression-free survival (PFS) of the combination of oral CB-839 (provided by Calithera Biosciences, South San Francisco, CA 94080) when administered with oral capecitabine. The secondary objectives are to determine the response rate and correlative studies. Pretreatment and on-treatment (10 to 14 days after initial treatment) liver tumor biopsies were taken by CT-guided needle biopsy. Response to therapy was assessed per RECIST 1.1 utilizing CT imaging obtained every 9 weeks. Patients were permitted to continue treatment until disease progression or development of unacceptable toxicity. All patients provided written informed consent prior to participating in the study. The trial was registered on clinicaltrials.gov (NCT02861300).

Eligibility: Patients were eligible for study entry if they had a colorectal cancer, had progressed on all standard lines of therapy, and must have progressed on prior fluoropyrimidine-based chemotherapy. Patients otherwise must have been at least 18 years of age, had an ECOG performance status of 0 or 1, had normal bone marrow, renal, and hepatic function, had the ability to swallow pills, and be able to understand and the willingness to sign consent. Patients were not eligible if they had ongoing treatment-related toxicities that were greater than grade 1, and they could not be receiving other investigational agents. Central nervous system involvement by their cancer or prior allergic reaction to either CB-839 or capecitabine was not permitted.

Statistics

GraphPad Prism software was used to create the graphs. Data are plotted as mean $\pm$ SEM. For two group comparison, we applied the t-test to compare the means between two groups, assuming unequal variances. For comparisons of more than 2 groups with a single variable, one-way ANOVA was used to assess for any significant differences across all groups, together with Dunnett's multiple pairwise comparison test to compare each pair for statistically significant difference between the pair. If the data have more than 1 variable, two-way ANOVA and Tukey's multiple pairwise comparison tests are used. For xenograft growth, we carried out two-way ANOVA for repeated measurements to test whether there is an overall difference in the tumor sizes by testing group differences as well as whether there was a difference in the development of tumor sizes over time between the 2 groups by testing the interaction between time and group. Kaplan-Meier analysis was used to assess differences in progression-free survival (PFS) stratified by levels changes of various biomarkers, generating a log-rank p-value as well as median survival time with 95% confidence intervals (95% CI). Patient response to therapy during the phase II clinical trial was defined per RECIST criteria. Patients were considered evaluable for response if they had measurable disease at the time of study entry, had received at least one cycle of therapy and had undergone a repeat disease evaluation with imaging. PFS was defined as the time from the beginning of treatment to RECIST evidence of progressive disease as determined by radiography or by clinical progression. $p < 0.05$ is defined as statistically significant.

Study approval

Animal experiments were approved by the Case Western Reserve University Animal Care and Use Committee. Both male and female mice were used in this study. The clinical trial was conducted with the approval of the Institutional Review Board and according to good clinical practice.

Data Availability

The RNA-seq were deposited into GEO (accession #: GSE245839). All other data are reported in the Supporting Data Value file.

Supplementary Methods include:

Somatic gene targeting
Intra-tumor injections
NK cell depletion
Macrophage depletion
Neutrophil depletion
Neutrophil isolation
Immunofluorescent staining
Quantification of immunostaining
In vitro netosis induction
RNA-seq
Cell death assays
Western blotting
Chromatin immunoprecipitation (ChIP)
Reactive oxygen species (ROS) measurement
ELISA assay
Cytokine array
Real-time PCR
RNA interference
In vitro protease cleavage assay

Author contributions

Z.W. conceived the project; ZW, YL, YZ, ES, SH, AH, RC, JEW designed the bench experiments; DB, and JE designed the phase II clinical trial; DB and AK led the clinical trial at Seidman Cancer Center and Taussig Cancer Center, respectively; YL and YZ, DJ, ES, GM, XZ, and ST performed the bench experiments; YL, SW, TD, SK, JEW, DB and ZW analyzed data; ES, JS, RL, BE, MS, SK, AM, SK, AK and DB recruited patients for the clinical trial. ZW, YL, DB and RC wrote the manuscript.

Acknowledgments

This work was supported by NIH grants R01CA196643, R01CA264320, R01CA260629, P50CA150964, and P30 CA043703. This work was also supported by a Stand Up to Cancer Colorectal Cancer Dream Team Translational Research Grant (Grant Number SU2C-AACR-DT22-17). Stand Up to Cancer is a program of the Entertainment Industry Foundation. Research grants are administered by the American Association for Cancer Research, a scientific partner of SU2C. Calithera Bioscience provided funding for the clinical trial and CB-839 for the clinical trial and for animal studies. We thank Dr. Sanford Markowitz for helpful discussions.

List of Supplementary Materials

Figures S1 to S10

Tables S1 to S5

References:

1. Burn GL, Foti A, Marsman G, Patel DF, and Zychlinsky A. The Neutrophil. *Immunity.* 2021;54(7):1377-91.
2. Brinkmann V, Reichard U, Goosmann C, Fauler B, Uhlemann Y, Weiss DS, et al. Neutrophil extracellular traps kill bacteria. *Science.* 2004;303(5663):1532-5.
3. Papayannopoulos V. Neutrophil extracellular traps in immunity and disease. *Nat Rev Immunol.* 2018;18(2):134-47.
4. Korkmaz B, Horwitz MS, Jenne DE, and Gauthier F. Neutrophil elastase, proteinase 3, and cathepsin G as therapeutic targets in human diseases. *Pharmacol Rev.* 2010;62(4):726-59.
5. Albrengues J, Shields MA, Ng D, Park CG, Ambrico A, Poindexter ME, et al. Neutrophil extracellular traps produced during inflammation awaken dormant cancer cells in mice. *Science.* 2018;361(6409).
6. Adrover JM, McDowell SAC, He XY, Quail DF, and Egeblad M. NETworking with cancer: The bidirectional interplay between cancer and neutrophil extracellular traps. *Cancer Cell.* 2023;41(3):505-26.
7. Vasan N, and Cantley LC. At a crossroads: how to translate the roles of PI3K in oncogenic and metabolic signalling into improvements in cancer therapy. *Nat Rev Clin Oncol.* 2022;19(7):471-85.
8. Samuels Y, Wang Z, Bardelli A, Silliman N, Ptak J, Szabo S, et al. High frequency of mutations of the PIK3CA gene in human cancers. *Science.* 2004;304(5670):554.
9. Hao Y, Samuels Y, Li Q, Krokowski D, Guan BJ, Wang C, et al. Oncogenic PIK3CA mutations reprogram glutamine metabolism in colorectal cancer. *Nat Commun.* 2016;7:11971.
10. Zhao Y, Feng X, Chen Y, Selfridge JE, Gorityala S, Du Z, et al. 5-Fluorouracil Enhances the Antitumor Activity of the Glutaminase Inhibitor CB-839 against PIK3CA-Mutant Colorectal Cancers. *Cancer Res.* 2020;80(21):4815-27.
11. Liu K, Sun E, Lei M, Li L, Gao J, Nian X, et al. BCG-induced formation of neutrophil extracellular traps play an important role in bladder cancer treatment. *Clin Immunol.* 2019;201:4-14.
12. Schedel F, Mayer-Hain S, Pappelbaum KI, Metze D, Stock M, Goerge T, et al. Evidence and impact of neutrophil extracellular traps in malignant melanoma. *Pigment Cell Melanoma Res.* 2020;33(1):63-73.
13. Wang CL, Wang Y, Jiang QL, Zeng Y, Yao QP, Liu X, et al. DNase I and Sivelestat Ameliorate Experimental Hindlimb Ischemia-Reperfusion Injury by Eliminating Neutrophil Extracellular Traps. *J Inflamm Res.* 2023;16:707-21.
14. Hao Y, He B, Wu L, Li Y, Wang C, Wang T, et al. Nuclear translocation of p85beta promotes tumorigenesis of PIK3CA helical domain mutant cancer. *Nat Commun.* 2022;13(1):1974.
15. Rot A. Chemotactic potency of recombinant human neutrophil attractant/activation protein-1 (interleukin-8) for polymorphonuclear leukocytes of different species. *Cytokine.* 1991;3(1):21-7.
16. Harada A, Kuno K, Nomura H, Mukaida N, Murakami S, and Matsushima K. Cloning of a cDNA encoding a mouse homolog of the interleukin-8 receptor. *Gene.* 1994;142(2):297-300.

17. Kucharzik T, Hudson JT, 3rd, Lugering A, Abbas JA, Bettini M, Lake JG, et al. Acute induction of human IL-8 production by intestinal epithelium triggers neutrophil infiltration without mucosal injury. *Gut.* 2005;54(11):1565-72.
18. Fan X, Patera AC, Pong-Kennedy A, Deno G, Gonsiorek W, Manfra DJ, et al. Murine CXCR1 is a functional receptor for GCP-2/CXCL6 and interleukin-8/CXCL8. *J Biol Chem.* 2007;282(16):11658-66.
19. Cacalano G, Lee J, Kikly K, Ryan AM, Pitts-Meek S, Hultgren B, et al. Neutrophil and B cell expansion in mice that lack the murine IL-8 receptor homolog. *Science.* 1994;265(5172):682-4.
20. Mihara K, Smit MJ, Krajnc-Franken M, Gossen J, Rooseboom M, and Dokter W. Human CXCR2 (hCXCR2) takes over functionalities of its murine homolog in hCXCR2 knockin mice. *Eur J Immunol.* 2005;35(9):2573-82.
21. Li Y, Liu Z, Zhao Y, Yang J, Xiao TS, Conlon RA, et al. PD-L1 expression is regulated by ATP-binding of the ERBB3 pseudokinase domain. *Genes Dis.* 2023;10(4):1702-13.
22. Zhang X, Chen X, Song H, Chen HZ, and Rovin BH. Activation of the Nrf2/antioxidant response pathway increases IL-8 expression. *Eur J Immunol.* 2005;35(11):3258-67.
23. An Z, Li J, Yu J, Wang X, Gao H, Zhang W, et al. Neutrophil extracellular traps induced by IL-8 aggravate atherosclerosis via activation NF-kappaB signaling in macrophages. *Cell Cycle.* 2019;18(21):2928-38.
24. Remijsen Q, Vanden Berghe T, Wirawan E, Asselbergh B, Parthoens E, De Rycke R, et al. Neutrophil extracellular trap cell death requires both autophagy and superoxide generation. *Cell Res.* 2011;21(2):290-304.
25. Branzk N, and Papayannopoulos V. Molecular mechanisms regulating NETosis in infection and disease. *Semin Immunopathol.* 2013;35(4):513-30.
26. Greco MN, Hawkins MJ, Powell ET, Almond HR, Jr., Corcoran TW, de Garavilla L, et al. Nonpeptide inhibitors of cathepsin G: optimization of a novel beta-ketophosphonic acid lead by structure-based drug design. *J Am Chem Soc.* 2002;124(15):3810-1.
27. El Rayes T, Catena R, Lee S, Stawowczyk M, Joshi N, Fischbach C, et al. Lung inflammation promotes metastasis through neutrophil protease-mediated degradation of Tsp-1. *Proc Natl Acad Sci U S A.* 2015;112(52):16000-5.
28. Yang L, Liu Q, Zhang X, Liu X, Zhou B, Chen J, et al. DNA of neutrophil extracellular traps promotes cancer metastasis via CCDC25. *Nature.* 2020;583(7814):133-8.
29. Sionov RV, Fainsod-Levi T, Zelter T, Polyansky L, Pham CT, and Granot Z. Neutrophil Cathepsin G and Tumor Cell RAGE Facilitate Neutrophil Anti-Tumor Cytotoxicity. *Oncoimmunology.* 2019;8(9):e1624129.
30. Nomura M, Shimizu S, Sugiyama T, Narita M, Ito T, Matsuda H, et al. 14-3-3 Interacts directly with and negatively regulates pro-apoptotic Bax. *J Biol Chem.* 2003;278(3):2058-65.
31. Zhao Y, Zhao X, Chen V, Feng Y, Wang L, Croniger C, et al. Colorectal cancers utilize glutamine as an anaplerotic substrate of the TCA cycle in vivo. *Sci Rep.* 2019;9(1):19180.
32. Singer M, and Sansonetti PJ. IL-8 is a key chemokine regulating neutrophil recruitment in a new mouse model of Shigella-induced colitis. *J Immunol.* 2004;173(6):4197-206.
33. Rajarathnam K, Schnoor M, Richardson RM, and Rajagopal S. How do chemokines navigate neutrophils to the target site: Dissecting the structural mechanisms and signaling pathways. *Cell Signal.* 2019;54:69-80.

34. Jia X, Wei S, and Xiong W. CXCL5/NF-kappaB Pathway as a Therapeutic Target in Hepatocellular Carcinoma Treatment. *J Oncol.* 2021;2021:9919494.
35. Hutti JE, Pfefferle AD, Russell SC, Sircar M, Perou CM, and Baldwin AS. Oncogenic PI3K mutations lead to NF-kappaB-dependent cytokine expression following growth factor deprivation. *Cancer Res.* 2012;72(13):3260-9.
36. Park J, Wysocki RW, Amoozgar Z, Maiorino L, Fein MR, Jorns J, et al. Cancer cells induce metastasis-supporting neutrophil extracellular DNA traps. *Sci Transl Med.* 2016;8(361):361ra138.
37. Gupta S, and Kaplan MJ. The role of neutrophils and NETosis in autoimmune and renal diseases. *Nat Rev Nephrol.* 2016;12(7):402-13.
38. Carminita E, Crescence L, Brouilly N, Altie A, Panicot-Dubois L, and Dubois C. DNAse-dependent, NET-independent pathway of thrombus formation in vivo. *Proc Natl Acad Sci U S A.* 2021;118(28).
39. Huang H, Tohme S, Al-Khafaji AB, Tai S, Loughran P, Chen L, et al. Damage-associated molecular pattern-activated neutrophil extracellular trap exacerbates sterile inflammatory liver injury. *Hepatology.* 2015;62(2):600-14.
40. Kinoshita M, Ogawa Y, Hama N, Ujiie I, Hasegawa A, Nakajima S, et al. Neutrophils initiate and exacerbate Stevens-Johnson syndrome and toxic epidermal necrolysis. *Sci Transl Med.* 2021;13(600).
41. Shinde-Jadhav S, Mansure JJ, Rayes RF, Marcq G, Ayoub M, Skowronski R, et al. Role of neutrophil extracellular traps in radiation resistance of invasive bladder cancer. *Nat Commun.* 2021;12(1):2776.
42. Mousset A, Lecorgne E, Bourget I, Lopez P, Jenovai K, Cherfils-Vicini J, et al. Neutrophil extracellular traps formed during chemotherapy confer treatment resistance via TGF-beta activation. *Cancer Cell.* 2023;41(4):757-75 e10.
43. Mehta HM, and Corey SJ. G-CSF, the guardian of granulopoiesis. *Semin Immunol.* 2021;54:101515.
44. Zhu CL, Xie J, Zhao ZZ, Li P, Liu Q, Guo Y, et al. PD-L1 maintains neutrophil extracellular traps release by inhibiting neutrophil autophagy in endotoxin-induced lung injury. *Front Immunol.* 2022;13:949217.
45. Zhao Y, Zhang X, Guda K, Lawrence E, Sun Q, Watanabe T, et al. Identification and functional characterization of paxillin as a target of protein tyrosine phosphatase receptor T. *Proc Natl Acad Sci U S A.* 2010;107(6):2592-7.

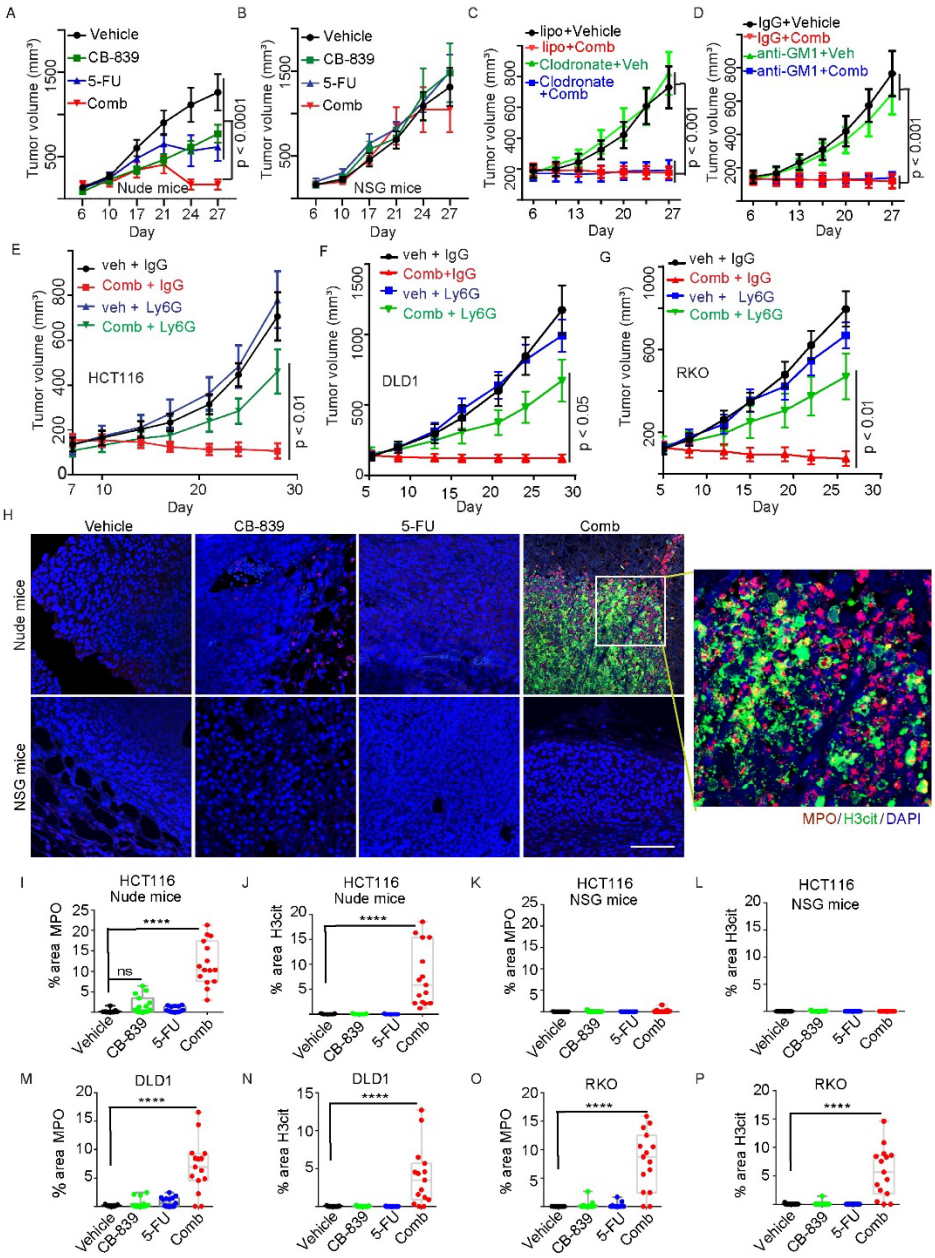

Figure 1. **The combination of CB-839 and 5-FU induces neutrophil extracellular traps (NETs) in xenograft tumors in nude mice**. (**A** & **B**) Xenograft tumors of HCT116 were treated with the indicated drugs five days on and two days off in nude and NSG mice simultaneously, with the growth curves shown in (A) nude mice and (B) NSG mice (5 mice/group). (**C** & **D**) Mice were implanted with HCT116 cells, and after 6 days, mice were injected with either 100 µl liposome control or clodronate twice a week (C), IgG control or anti-GM1 twice a week (D), growth curves shown in (C) for macrophage depletion and (D) for NK cell depletion (5 mice/group). Mice were treated CB-839, 5-FU, and the drug combination daily continuously. (**E** to **G**) CRC xenograft tumors treated with vehicle or drug combination with or without Ly6g antibody injection, tumor sizes were measured, and growth curves are shown in (E) for HCT116, (F) for DLD1, and (G) for RKO (5 mice/group). **(H-L)** Tumors shown in (A) & (B) were stained with antibodies against myeloperoxidase (MPO), which marks neutrophils and NETs, and citrullinated histone H3 (H3cit), which marks NETs. Representative images are shown in (H, scale bar: 50 µm), and quantifications are shown in (I to L), (n=15/group). (**M** to **P**) Tumors treated with the indicated drugs were stained with antibodies against MPO or H3cit and quantified (n=15/group). The growth curves of the drug treatment were published in (10). Data in (A) to (G) are plotted as mean ± SEM. Two-way ANOVA (A-G) or One-way ANOVA (I-P) was used for statistical analysis. *p<0.05; **p<0.01; ***p<0.001; ****p<0.0001.

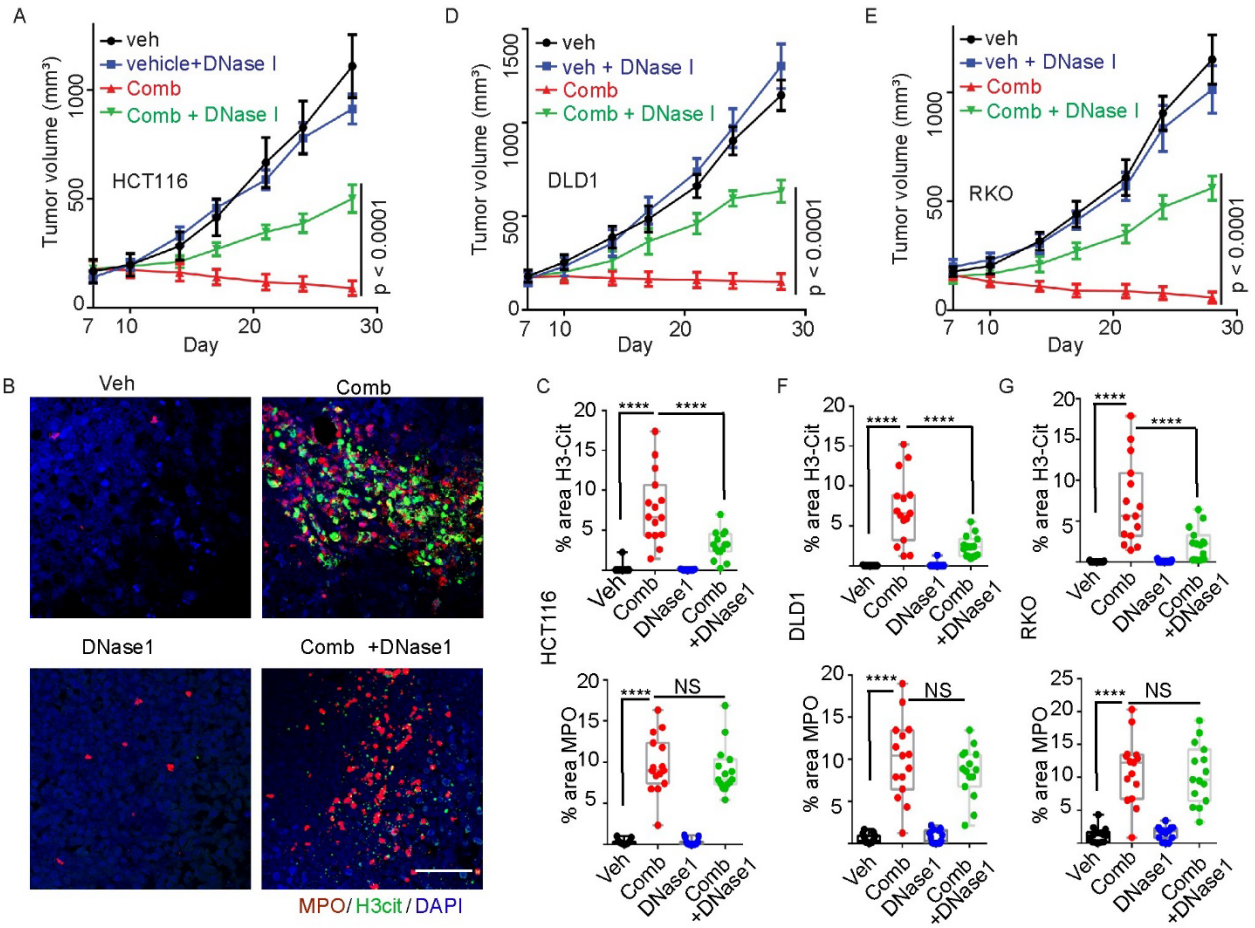

Figure 2. Disruption of NETs by DNase I treatment or depletion of neutrophils attenuates the tumor-inhibitory effect of the combination of CB-839 and 5-FU. (**A** to **G**) The indicated xenograft tumors in nude mice were treated with vehicle (Veh) or the drug combination (Comb) with or without DNase I (5 mice/group). Tumor growth curves are shown in (A), (D), & (E). Tumors were stained with antibodies against MPO and H3cit. Representative images of HCT116 tumors are shown in (B). Quantifications are shown in (C), (F), & (G). (n=15/group). Scale bar: 50 µm. Two-way ANOVA (A, D & E) or one-way ANOVA (C, F & G) was used for statistical analysis. *p<0.05; **p<0.01; ***p<0.001; ****p<0.0001.

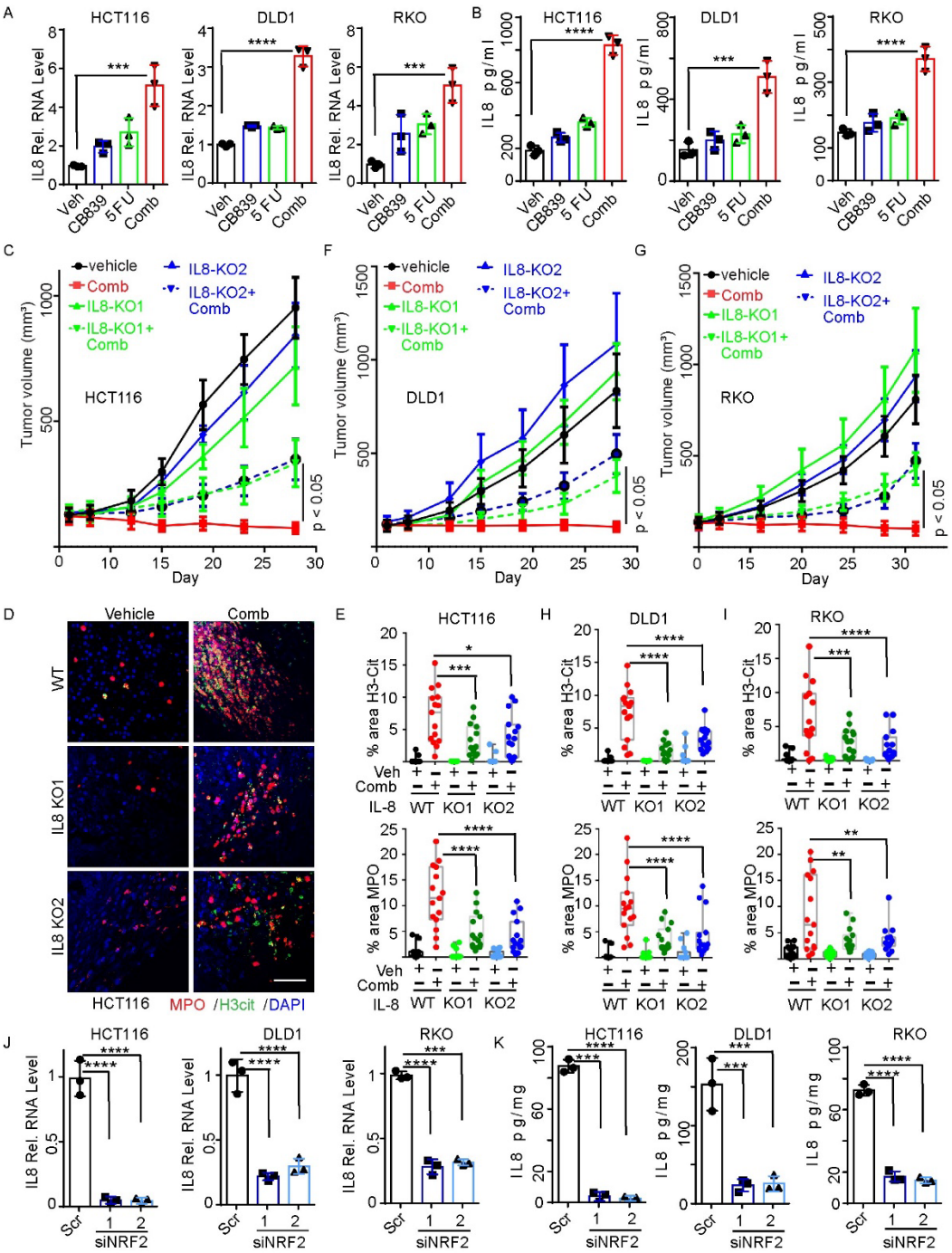

Figure 3. The combination of CB-839 and 5-FU induces IL-8 expression in CRCs to attract tumor-infiltrating neutrophils. (**A** & **B**) The indicated cells were treated with the indicated drugs. IL-8 mRNA and protein levels were measured by qRT-PCR (A) and ELISA (B), respectively, (n=3/group). (**C** to **I**) Parental HCT116, DLD1, RKO, and their *IL-8* KO clones were grown as xenograft tumors in nude mice and treated with vehicle or the combination of CB-839 and 5-FU (5 mice/group). Tumor growth curves are shown in (C), (F), & (G). Tumors were stained with antibodies against MPO and H3cit. Representative images of HCT116 tumors are shown in (D). Quantifications are shown in (E), (H) & (I), (n=15/group). (**J** & **K**) The indicated CRC cells were transfected with scramble siRNA or two independent siRNA against IL-8. IL-8 mRNA levels are shown in (J), and secreted IL-8 levels are shown in (K), (n=3/group). Scale bar: 50 μm. Two-way ANOVA (C, F & G, E, H & I) or one-way ANOVA (A & B, J & K) was used for statistical analysis. *p<0.05; **p<0.01; ***p<0.001; ****p<0.0001.

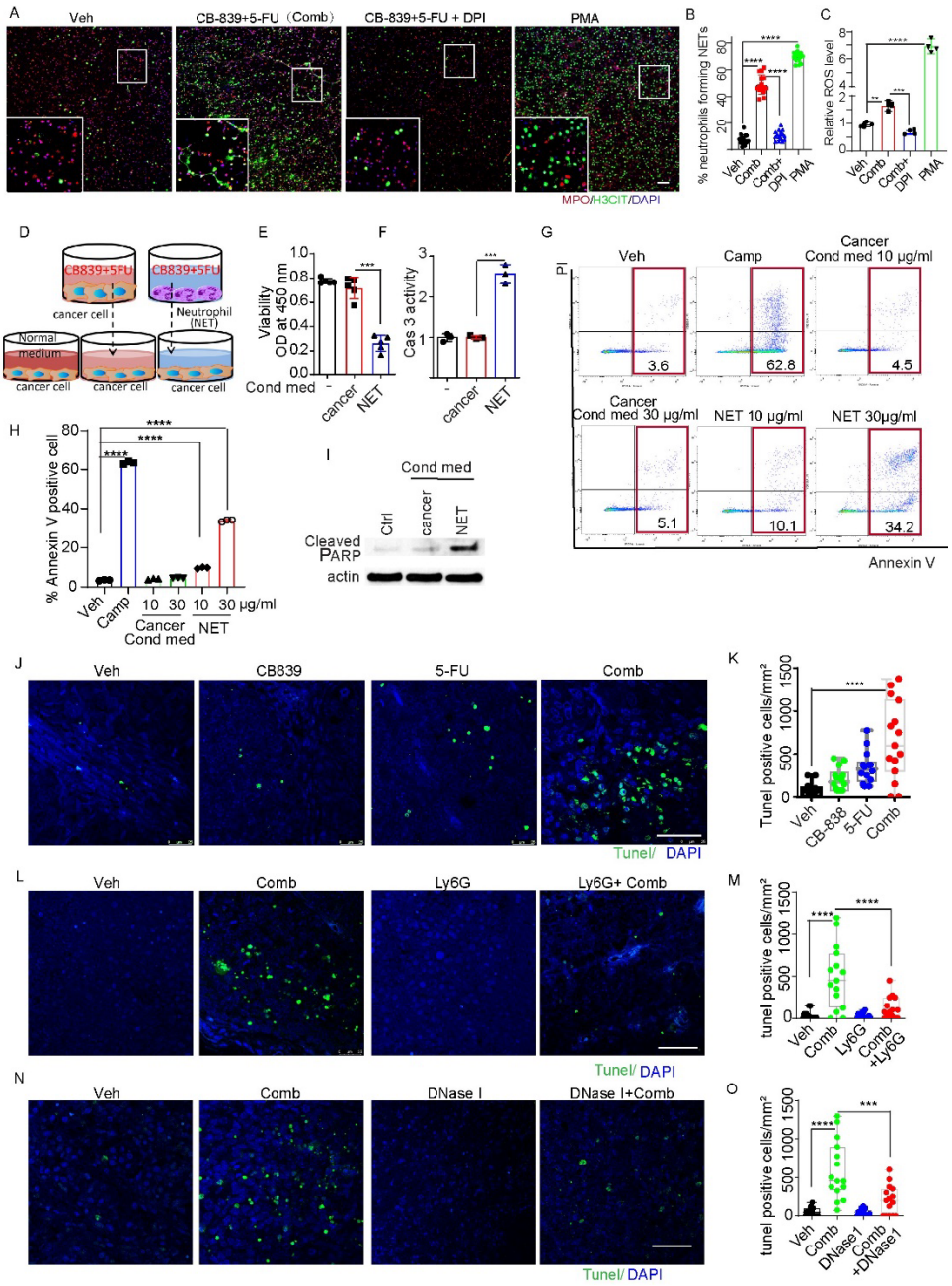

Figure 4. The combination of CB-839 and 5-FU acts on neutrophils to induce NET and causes apoptosis in cancer cells. (**A** to **C**) Purified neutrophils were treated with the indicated compounds and stained with antibodies against MPO and H3cit. Representative images are shown in (A), and quantifications are shown in (B), (n=15/group). The levels of ROS are shown in (C) (n=4/group). Diphenyleneiodonium (DPI, 2 μM) is a ROS scavenger. Neutrophils were treated with phorbol myristate acetate (PMA, 1 μM) as a positive control. (**D** to **I**) (D) Schematics of the experiment setup. Cancer cells or neutrophils (NET) were treated with the combination of CB-839 and 5-FU, the conditioned media were collected, and protein concentrations of the conditioned media were measured. The indicated conditioned media were diluted to a final concentration of 10 μg/ml, or 30 μg/ml in fresh McCoy's 5A medium to treat HCT116 cancer cells overnight. Cell viabilities are shown in (E) (n=5/group), caspase 3 activities are shown in (F) (n=3/group), annexin V positive cells are shown in (G & H), (n=3/group) and cleaved PARPs are shown in (I). HCT116 cells were treated with camptothecin (3 μM) as a positive control. (**J** to **O**) Tunel staining was performed on the HCT116 xenograft tumors with indicated treatment. Representative images of HCT116 tumors are shown in (J), (L), and (N), and quantifications are shown in (K), (M), and (O) (n=15/group). Scale bar: 50 μm. One-way ANOVA (B & C, E & F, H, K, M & O) was used for statistical analysis. *p<0.05; **p<0.01; ***p<0.001; ****p<0.0001.

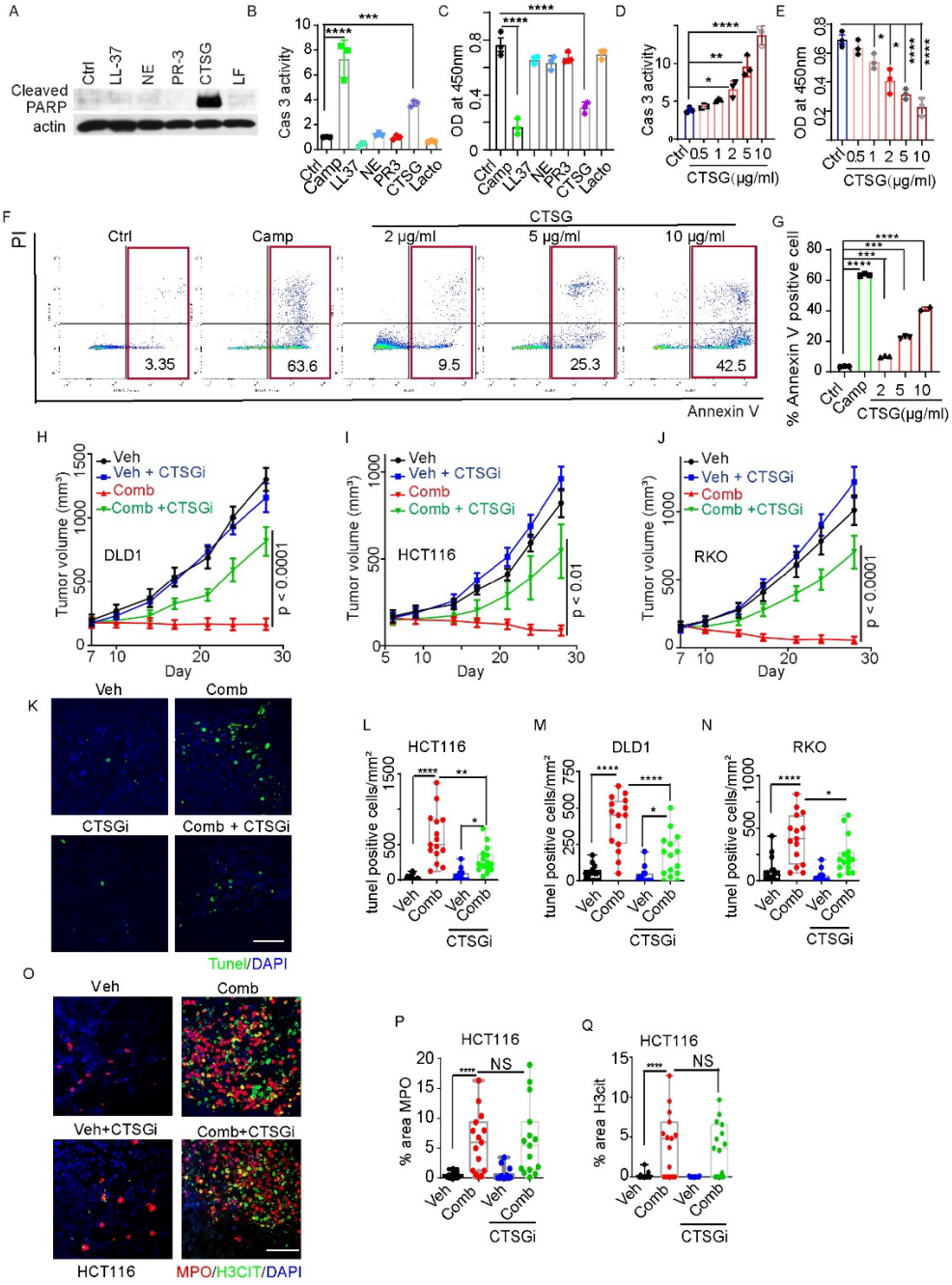

Figure 5. Cathepsin G (CTSG) in NETs inhibits tumor growth. (**A** to **C**) The HCT116 CRC cells were treated with the indicated recombinant proteins (10 μg/ml) overnight. Cell lysates were blotted with the indicated antibodies (A). The HCT116 cells were treated with the indicated recombinant proteins. Cells were treated with camptothecin (3 μM) in parallel as a positive control. Caspase 3 activities were measured (B) (n=3/group). Cell numbers are shown in (C) (n=3/group). (**D to G**) HCT116 cells were treated with indicated concentrations of recombinant CTSG. Caspase 3 activities are shown in (D) (n=3/group), Cell numbers were counted in E (n=3/group). Annexin V staining, and quantifications are shown in (F & G) (n=3/group). (**H** to **J**) The indicated xenograft tumors were established in nude mice and treated with vehicle or the drug combination with or without CTSGi (intratumor injection, 5 mice/group). (**K** to **N**) Tunel staining of the tumors is shown in (H-J). Representative images of HCT116 tumors are shown in (K). Quantifications are shown in (L to N) (n=15/group). **(O to Q)** Tumors from H stained with anti-MPO and anti-H3cit antibodies. Representative images of HCT116 tumors are shown in (O), and quantifications are shown in (P & Q) (n=15/group). Scale bar: 50 μm. One-way ANOVA (B to E, G, L to N, P & Q) or two-way ANOVA (H to J) was used for statistical analysis. *p<0.05; **p<0.01; ***p<0.001; ****p<0.0001.

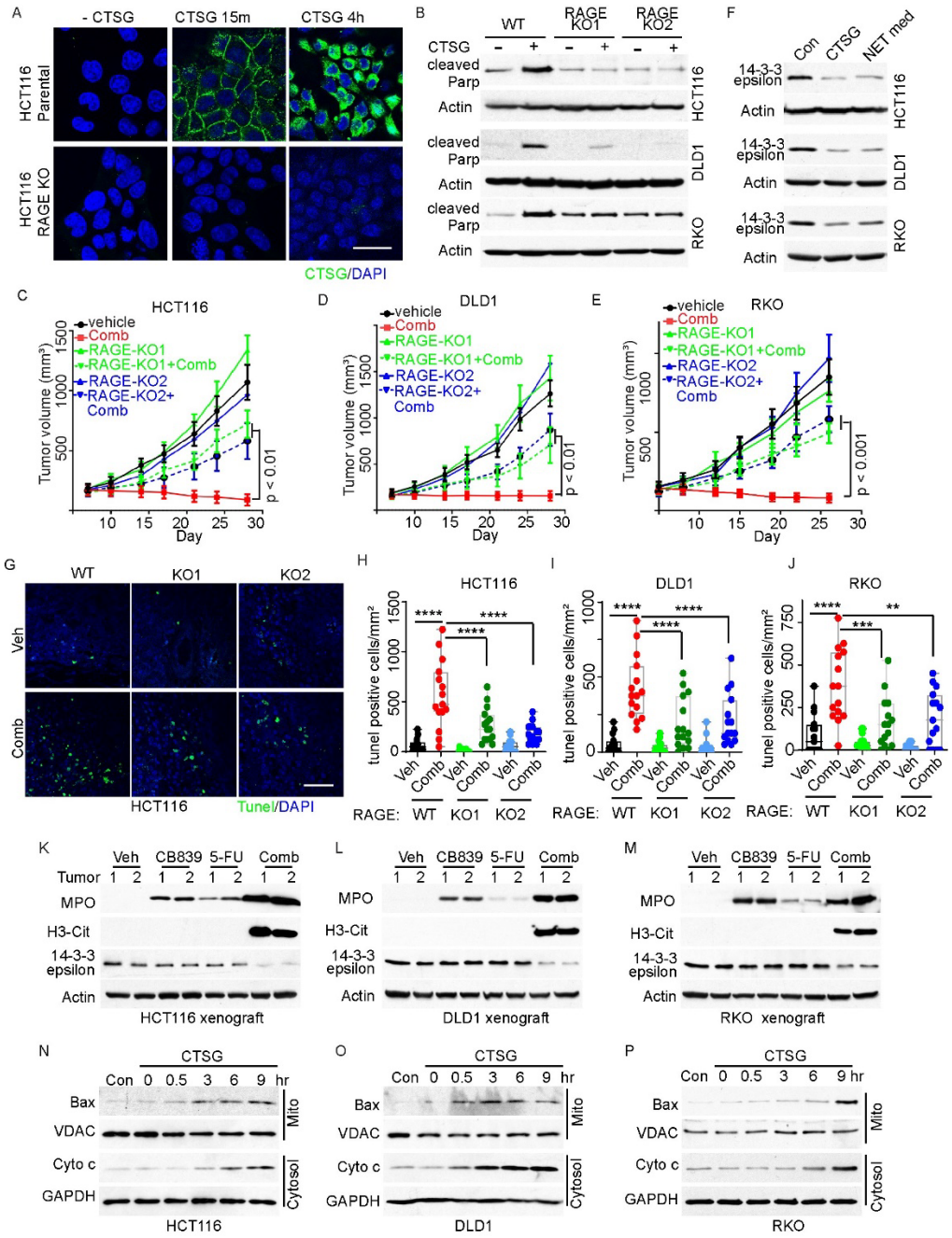

Figure 6. CTSG enters cancer cells through RAGE, cleaves 14-3-3ε, results in BAX mitochondrial translocation, and triggers apoptosis. (**A** & **B**) Parental HCT116, DLD1, RKO, and their RAGE KO cells were incubated with 5μg/ml recombinant CTSG for the indicated time. Representative images of immunofluorescent staining of an anti-CTSG antibody are shown in (A), and Western blots of cleaved PARP are shown in (B). (**C** to **E**) CRC RAGE WT and knockout tumors treated with vehicle or drug combination, tumor growth curves are shown in (C) for HCT116), (D) for DLD1, and (E) for RKO (5 mice/group). (**F**) CRC cells were treated with recombinant CTSG or NET-conditioned medium for 16 hours, and cell lysates were blotted with indicated antibodies. Corrected loading control provided. **(G to J)** Tunel staining was performed on the CRC xenograft tumors from (C) to (E). Representative images of HCT116 tumors are shown in (G), and quantifications are shown in (H) for HCT116, (I) for DLD1, and (J) for RKO (n=15/group). (**K** to **M**) Western blot of 14-3-3ε protein levels in the tumors with indicated treatment. (**N** to **P**) CRC cells were treated with 5μg/ml CTSG for the indicated time, and mitochondrial and cytosolic fractions were extracted by a cell fractionation kit and blotted with the indicated antibodies. Two-way ANOVA (C to E, H to J) was used for statistical analysis. *p<0.05; **p<0.01; ***p<0.001; ****p<0.0001.

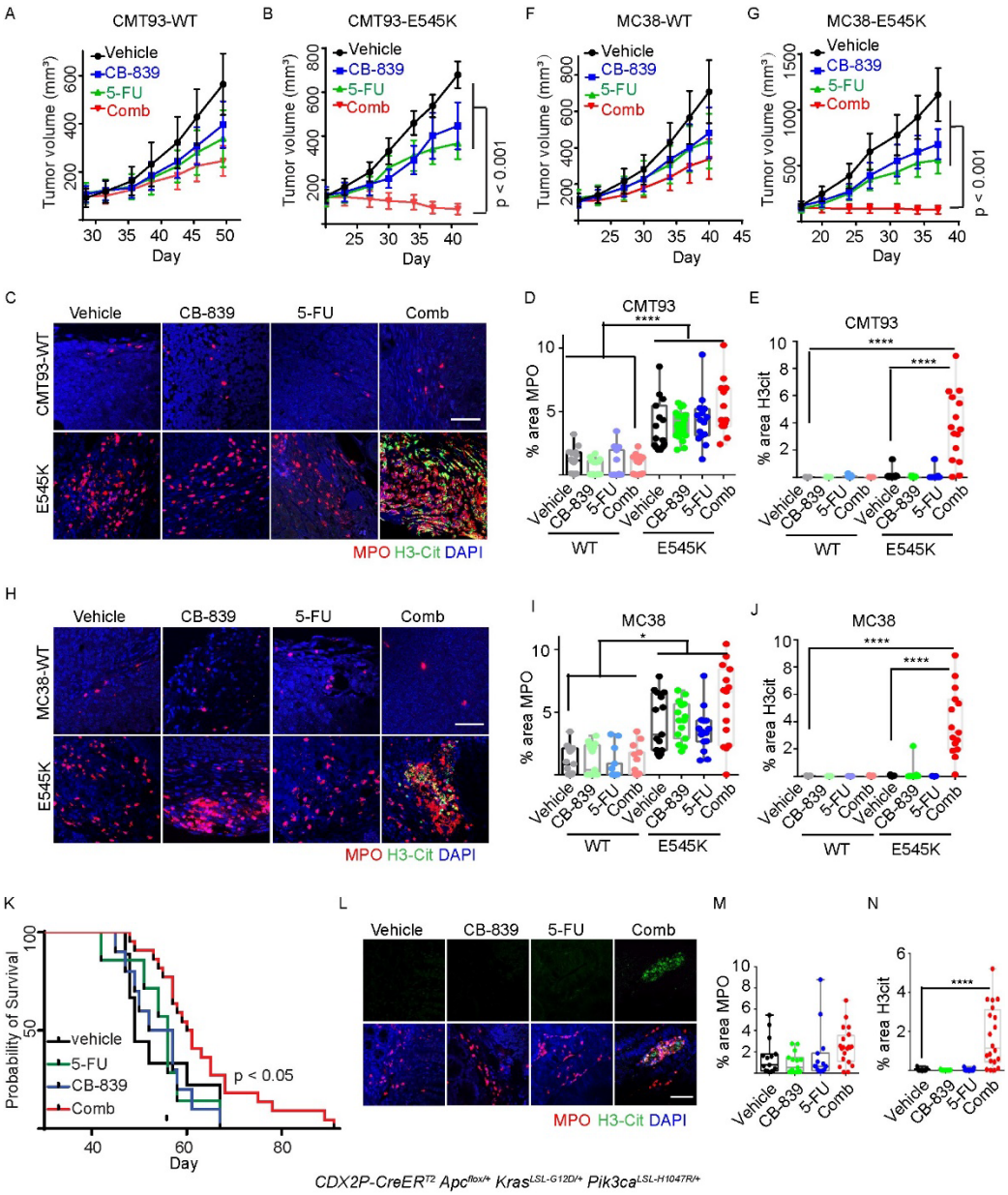

Figure 7. The combination of CB-839 and 5-FU induces NETs in syngeneic and genetically engineered mouse (GEM) *Pik3ca* mutant tumor models. (**A** & **B**) CMT93 *Pik3ca* WT or E545 K mutant tumors were treated with indicated drugs, with growth curves shown in (A) for CMT93 *Pik3ca* WT and (B) for CMT93 *Pik3ca* E545K mutant. (5 mice/group). (**C** to **E**) The indicated tumors were stained with antibodies against MPO and H3cit. Representative images are shown in (C). Quantifications shown in (D) and (E), (n=15/group). (**F** & **G**) MC38 *Pik3ca* WT or mutant tumors with indicated treatment, growth curve shown in (F) for MC38 *Pik3ca* WT, (G) for MC38 *Pik3ca* mutant (5 mice/group). (**H** to **J**) The indicated tumors were stained with antibodies against MPO and H3cit. Representative images are shown in (H). Quantifications shown in (I) and (J), (n=15/group). (**K**) *CDX2P-CreER*^{T2} *Apc*$^{flox/+}$ *Kras*$^{LSL-G12D/+}$ *Pik3ca*$^{LSL-H1047R/+}$ mice were treated with tamoxifen and then treated with the indicated drug a week post-tamoxifen treatment for four weeks. Kalplan-Meier curves of the mice are shown. A log-rank test was used to assess the statistical significance between the vehicle and the combination of CB-839 and 5-FU treatment groups. (**L** to **N**) *CDX2P-CreER*^{T2} *Apc*$^{flox/+}$ *Kras*$^{LSL-G12D/+}$ *Pik3ca*$^{LSL-H1047R/+}$ mice were treated with tamoxifen, and four weeks later, the mice were treated with the indicated drugs, and colon tumors were harvested and stained with antibodies against MPO and H3cit (3 mice/group). Representative images are shown in (L). Quantifications of MPO are shown in (M). Quantifications of H3cit are shown in (N), (n=15/group). Two-way ANOVA (A & B, D to G, I & J) or one-way ANOVA (N) was used for statistical analysis. *p<0.05; **p<0.01; ***p<0.001; ****p<0.0001. Scale bar: 50 μm.

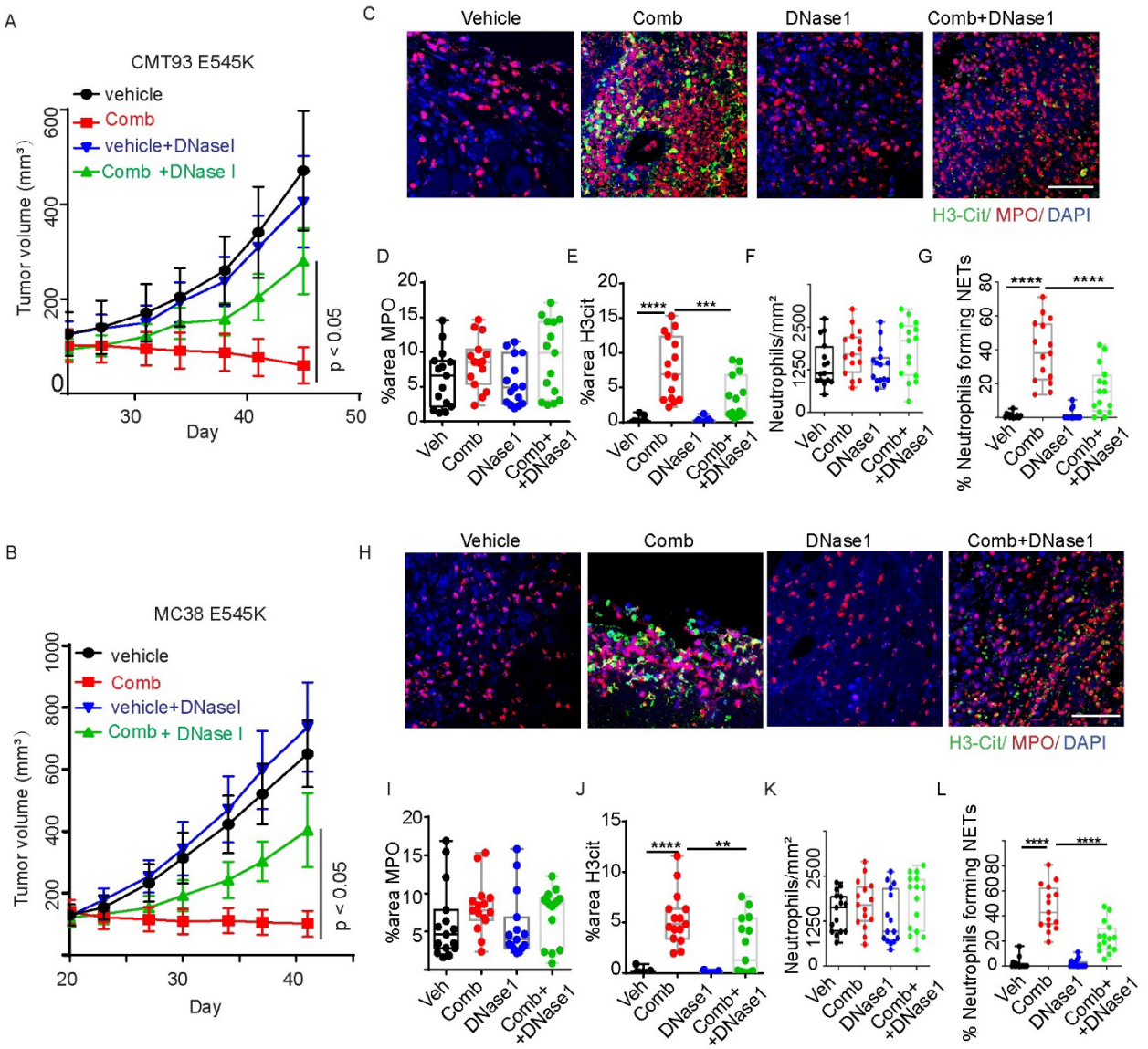

Figure 8. Disruption of NETs in syngeneic mouse tumors attenuates the tumor-inhibitory effect of the combination of CB-839 and 5-FU.

The indicated syngeneic tumors in C57/BL6 mice were treated with vehicle (Veh), or the drug combination (Comb) with or without DNase I. Tumor growth curves are shown in (**A**) for CMT93 *Pik3ca* E545K mutant tumors & (**B**) for MC38 *Pik3ca* E545K mutant tumors (5 mice/group), respectively. Tumors were stained with antibodies against MPO and H3cit. Representative images are shown in (**C**) for CMT93 *Pik3ca* E545K tumors and (**H**) for MC38 *Pik3ca* E545K tumors, respectively. Quantifications are shown in (**D** to **G**) for CMT93 *Pik3ca* E545K tumors and (**I** to **L**) for MC38 *Pik3ca* E545K tumors, respectively (n=15/group). Scale bar: 50 μm. Two-way ANOVA (A & B**)** or one-way ANOVA **(**D to G, I to L) was used for statistical analysis. *p<0.05; **p<0.01; ***p<0.001; ****p<0.0001.

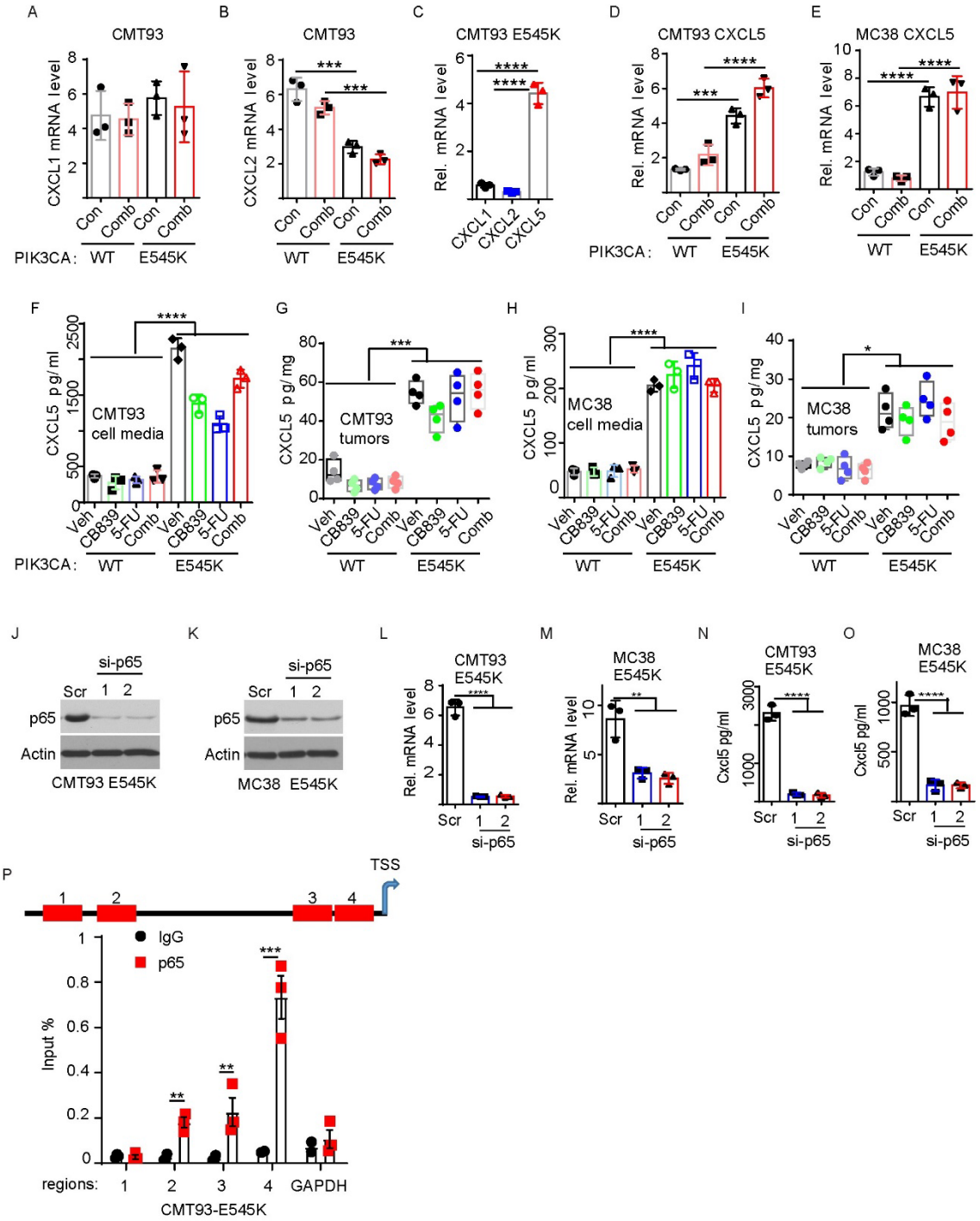

Figure 9. *Pik3ca* E545K mutation upregulates CXCL5 in mouse CRC cells. (**A & B**) RT-PCR of CXCL1 and CXCL2 levels in CMT93 *Pik3ca* WT and Mutant cells with the indicated treatment overnight (n=3/group). (**C**) RT-PCR of CXCL1, CXCL2, and CXCL5 in CMT93 E545K cells (n=3/group). (**D** & **E**) RT-PCR of CXCL5 in *Pik3ca* WT and E545K cells. D for CMT93, E for MC38 (n=3/group). (**F** to **I**) CXCL5 protein level in culture medium (F & G) and tumors (H & I) was measured by ELISA (n=3/group for F & H, n=4/group for G & I). (**J to O**) p65 was knocked down by two independent siRNA. Cell lysates were blotted with the indicated antibodies (J & K). CXCL5 mRNA levels were measured by qRT-PCR (L & M). Secreted CXCL5 was measured by ELISA (N & O) (n=3/group). (**P**) CMT93 *Pik3ca* mutant cells were treated with the combination of CB-839 and 5-FU. ChIP-PCRs were performed (n=3/group). Two tailed t test for (P), two-way ANOVA (B, D to I) or one-way ANOVA (C, L to O) was used for statistical analysis. *p<0.05; **p<0.01; ***p<0.001; ****p<0.0001.

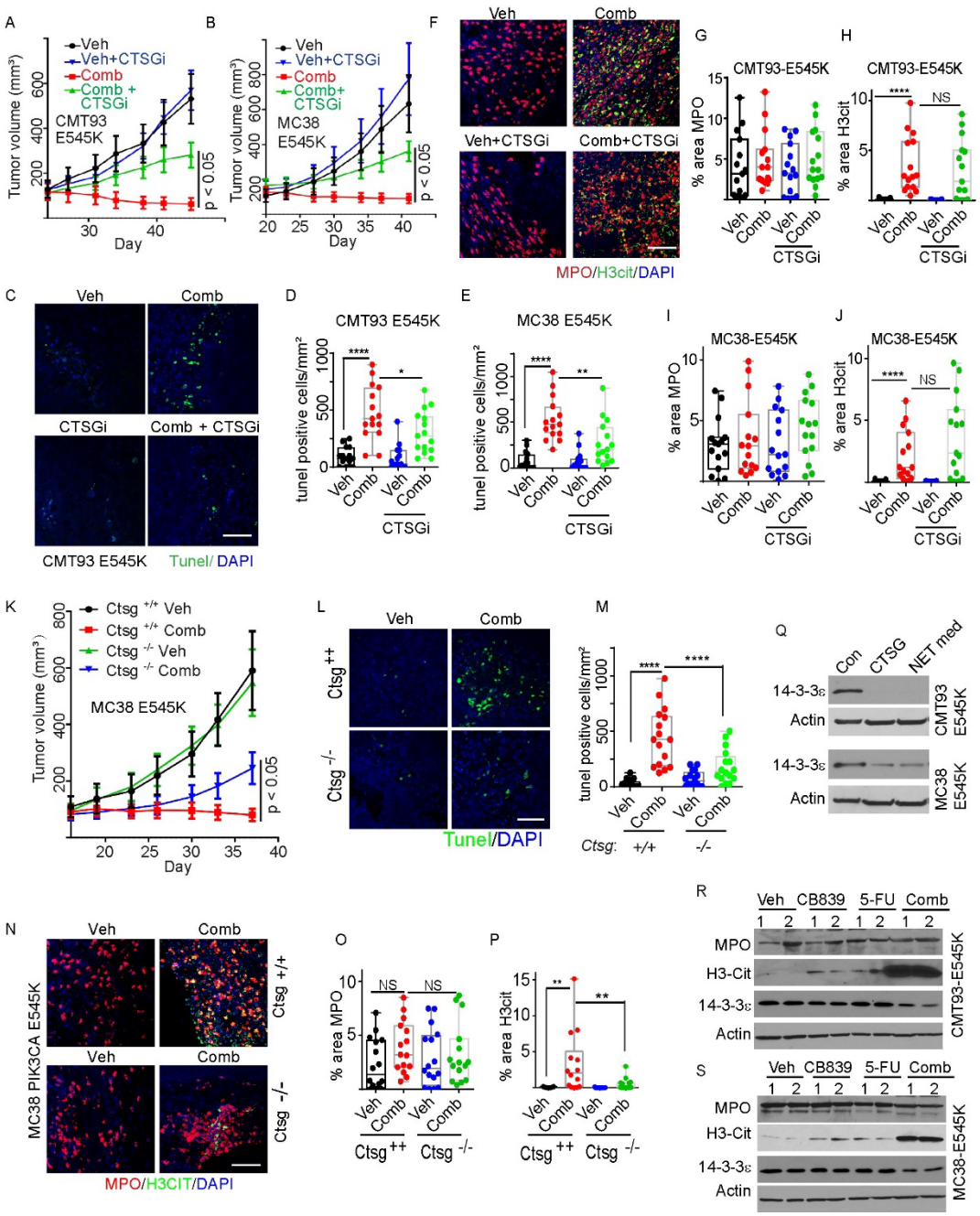

Figure 10. Cathepsin G (CTSG) in NETs induces apoptosis in the syngeneic model. (A & B) The indicated syngeneic tumors were treated with vehicle or the drug combination with or without CTSGi (5 mice/group). Growth curves are shown in (A & B). **(C-E)** Tunel staining was performed on the syngeneic tumors from (A & B). Representative images of CMT93 tumors are shown in (C), and quantifications are shown in (D & E) (n=15/group), (**F-J**) Tumors from A & B were stained with antibodies against MPO and H3cit (F) and quantified (G to J). (**K to M**) MC38 *Pik3ca* E545K mutant cells were injected into C57/Bl6 mice of the indicated genotypes and treated with vehicle or the combination of CB-839 and 5-FU (5 mice/group). The growth curves are shown in (K). Tunel staining was performed on the syngeneic tumors; representative images are shown in (L), and quantifications are shown in (M). (**N to P**) The tumors shown in (K) were stained with antibodies against MPO and H3cit. Representative images are shown in (N). quantifications are shown in (O & P) (n=15/group). (**Q**) mouse CRC cells treated with CTSG and NET medium for 16 hours, cell lysates were harvested and blotted with indicated antibodies. **(R & S)** tumors shown in A & B were blotted with indicated antibodies. Two-way ANOVA (A & B, K, M & P) or one-way ANOVA (D & E, H & J) was used for statistical analysis. *p<0.05; **p<0.01; ***p<0.001; ****p<0.0001.

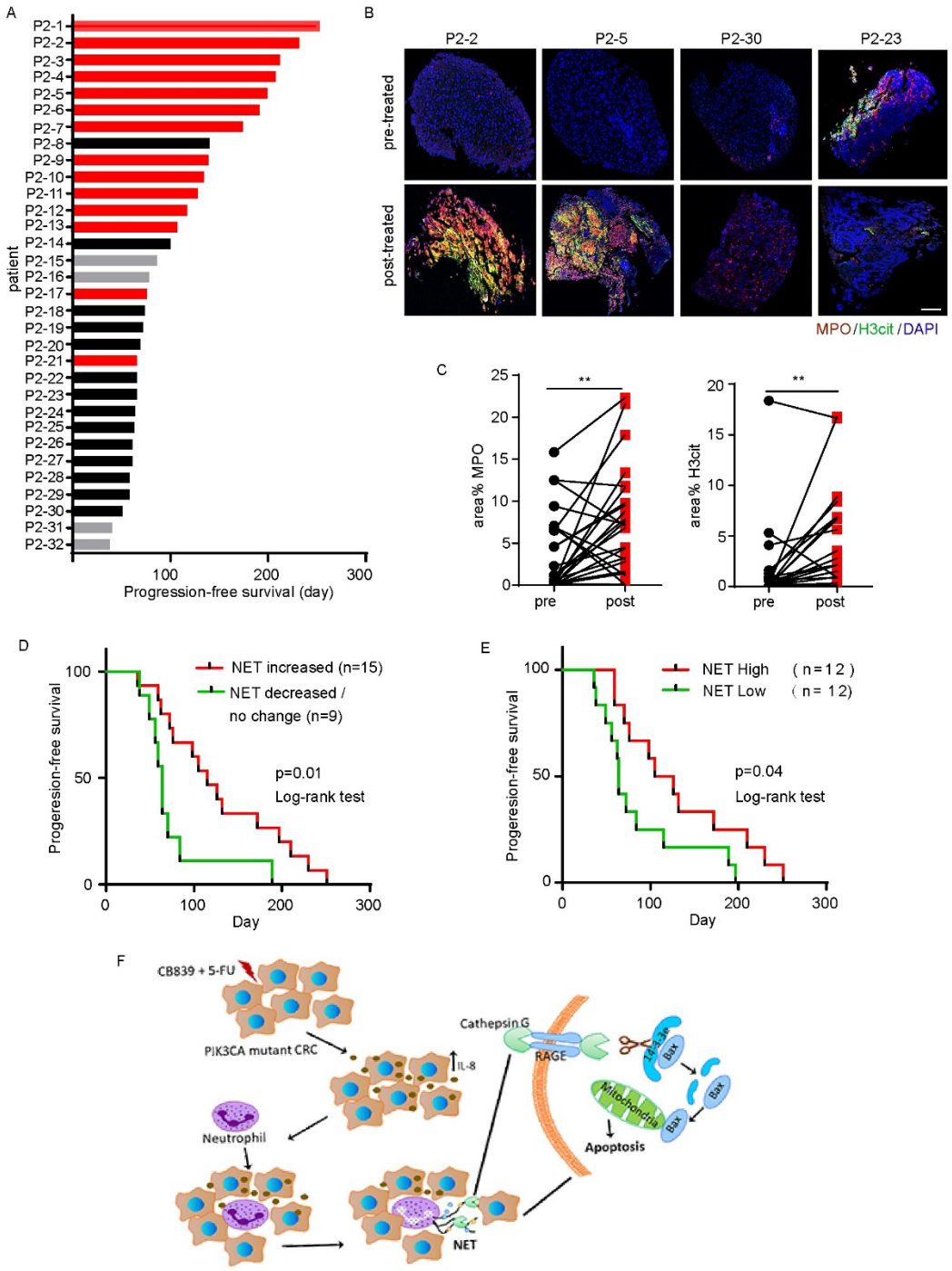

Figure 11. Higher tumor NET levels are associated with longer progression-free survival (PFS).
(**A**) PFS of 32 metastatic *PIK3CA* mutant CRC patients in a phase II clinical trial of the combination of CB-839 and capecitabine, an oral prodrug of 5-FU. Red bars: stable disease; black bars: progressive disease; and gray bars: not evaluable. (**B** & **C**) Tumor biopsies were stained with anti-MPO and anti-H3cit antibodies. Representative images are shown in (B), and quantifications are shown in (C). ** $p<0.01$; paired students t-test, two-tailed. Scale bar: 100 μM. (**D**) Kaplan-Meier curves of progression-free survival (PFS) of patients are plotted with increased levels of H3cit in posttreatment biopsies compared to pretreatment biopsies vs decreased levels of H3cit levels in posttreatment biopsies compared to pretreatment biopsies. (**E**) Kaplan-Meier plot of PFS of patients whose posttreatment biopsies with high levels of H3cit vs those with low levels of H3cit. (**F**) A model of CB-839 plus 5-FU-induced NETs, which release cathepsin G, enter cancer cells, cleave 14-3-3ε, lead to BAX mitochondrial translocation, and trigger apoptosis.